

**Data supporting the North Atlantic Climate System: Integrated Studies (ACSIS) programme,
including atmospheric composition, oceanographic and sea ice observations (2016-2022) and
output from ocean, atmosphere, land and sea-ice models (1950-2050)**

Alex T. Archibald^{1,2}, Bablu Sinha³, Maria R. Russo^{1,2}, Emily Matthews⁵, Freya A. Squires⁶, N. Luke Abraham^{1,2}, Stephane J.-B Bauguitte⁴, Thomas. J. Bannan⁵, Thomas G. Bell⁷, David Berry⁸, Lucy J. Carpenter⁹, Hugh Coe^{5,10}, Andrew Coward³, Peter Edwards^{9,11}, Daniel Feltham¹², Dwayne Heard¹³, Jim Hopkins^{9,11}, James Keeble^{1,2}, Elizabeth C. Kent³, Brian A. King³, Isobel R. Lawrence^{14,15}, James Lee^{9,15}, Claire R. Macintosh¹⁶, Alex Megann³, Bengamin I. Moat³, Katie Read^{9,11}, Chris Reed⁴, Malcolm J. Roberts¹⁷, Reinhard Schiemann¹⁸, David Schroeder¹², Timothy J. Smyth⁷, Loren Temple⁹, Navaneeth Thamban⁵, Lisa Whalley^{13,19}, Simon Williams³, Huihui Wu⁵, Mingxi Yang⁷

Deleted: -x

¹National Centre for Atmospheric Science, University of Cambridge, Cambridge, United Kingdom

²Yusuf Hamied Department of Chemistry, University of Cambridge, Cambridge CB2 1EW, United Kingdom

³National oceanography Centre, United Kingdom.

⁴Facility for Airborne Atmospheric Measurements Airborne Laboratory, Cranfield University, Cranfield MK43 0AL, United Kingdom

⁵Department of Earth and Environmental Science, Centre for Atmospheric Science, University of Manchester, Manchester M13 9PL, United Kingdom

⁶British Antarctic Survey, Cambridge CB3 0ET, United Kingdom

⁷Plymouth Marine Laboratory, Plymouth PL1 3DH, United Kingdom

⁸WMO, Geneva, Switzerland

⁹Wolfson Atmospheric Chemistry Laboratories, Department of Chemistry, University of York, York YO10 5DD, United Kingdom

¹⁰National Centre for Atmospheric Science, University of Manchester, Manchester M13 9PL, United Kingdom

¹¹National Centre for Atmospheric Science, University of York, York, United Kingdom

¹²CPOM, University of Reading, Reading, UK

¹³School of Chemistry, University of Leeds, Leeds LS2 9JT, United Kingdom

¹⁴ESA ESRIN, Via Galileo Galilei, 1, 00044 Frascati RM, Italy.

¹⁵CPOM, University of Leeds, Leeds, United Kingdom

¹⁶ESA Climate Office, United Kingdom

¹⁷Met Office Hadley Centre, Exeter, UK.

¹⁸National Centre for Atmospheric Science, Department of Meteorology, University of Reading, Reading, UK

¹⁹National Centre for Atmospheric Science, University of Leeds, Leeds, United Kingdom

Correspondence to: Alex Archibald (ata27@cam.ac.uk) and Bablu Sinha (bablu@noc.ac.uk)

Abstract. The North Atlantic Climate System: Integrated Study (ACSIS) was a large multidisciplinary research programme funded by the United Kingdom's Natural Environment Research Council (NERC). ACSIS ran from 2016-22 and brought together around 80 scientists from seven leading UK-based environmental research institutes to deliver major advances in understanding North Atlantic climate variability and extremes. Here we present an overview of the data generated by the ACSIS programme. The datasets [described here](#) cover the North Atlantic Ocean, the atmosphere above it including its composition, and Arctic Sea Ice,

Atmospheric composition datasets include measurements from 7 aircraft campaigns ([45 flights in total](#), 0-10km altitude range) in the north eastern Atlantic (~40°W-5°E, ~15°N-55°N) made at intervals of from 6 months to 2 years between February 2017 and [May 2022](#). The flights measured chemical species (including greenhouse gases, ozone precursors and VOCs) and aerosols (organic, SO₄, NH₄, NO₃, and nss-Cl) (<https://dx.doi.org/10.5285/6285564c34a246fc9ba5ce053d85e5e7> (FAAM et al. (2024))). Ground based stations at the Cape Verde Atmospheric Observatory (CVAO), Penlee Point Atmospheric Observatory (PPAO) and Plymouth Marine Laboratory (PML) recorded ozone, ozone precursors, halocarbons, as well as greenhouse gases (CO₂, methane), SO₂ and photolysis rates. (CVAO, <http://catalogue.ceda.ac.uk/uuid/81693aad69409100b1b9a247b9ae75d5>, National Centre for Atmospheric Science et al. (2014)), O₃ and CH₄ (PPAO, <https://catalogue.ceda.ac.uk/uuid/8f1ff8ea77534e08b03983685990a9b0> (Plymouth Marine Laboratory and Yang (2024)) and aerosols (PML, <https://dx.doi.org/10.5285/e74491c96ef24df29a9342a3d57b5939>, Smyth (2024))).

Complementary model simulations of atmospheric composition were performed with the UK Earth System Model, UKESM1, for the period 1982 to 2020 using CMIP6 historical forcing up to 2014 and SSP3-7.0 scenario from 2015-2020. Model temperature and winds were relaxed towards ERA reanalysis. Monthly mean model data for ozone, NO, NO₂, CO, methane, stratospheric ozone tracers and 30 regionally emitted tracers are available to download (<https://data.ceda.ac.uk/badc/acsis/UKESM1-hindcasts>, Abraham (2024)).

ACSIS also generated new ocean heat content diagnostics <https://doi.org/10/g6wm>, <https://doi.org/10/g8g2>, Moat et al. (2021a-b) and gridded temperature and salinity based on objectively mapped Argo measurements <https://doi.org/10.5285/fe8e524d-7f04-41f3-e053-6c86abc04d51> (King (2023)).

Deleted: the full North Atlantic System comprising:

Deleted: and the Greenland Ice Sheet

Deleted: between 3 and 10 flights each

Deleted: m

An ensemble of atmosphere-forced global ocean-sea ice simulations using the NEMO-CICE model was performed with horizontal resolutions of $1/4^\circ$ and $1/12^\circ$ covering the period 1958-2020 using several different atmosphere reanalysis based surface forcing datasets, supplemented by additional global simulations and standalone sea ice model simulations with advanced sea ice physics using the CICE model (<http://catalogue.ceda.ac.uk/uuid/770a885a8bc34d51ad71e87ef346d6a8>, Megann et al. (2021e)). Output is stored as monthly averages and includes 3D potential temperature, salinity, zonal, meridional and vertical velocity; 2D sea surface height, mixed layer depth, surface heat and freshwater fluxes, ice concentration and thickness and a wide variety of other variables.

In addition to the data presented here we provide a [very](#) brief overview of several other datasets that were generated during ACSIS [and](#) have been described previously in the literature.

Deleted: which

1. The North Atlantic Climate System

The North Atlantic Climate System Integrated Study (ACSIS) was a 6-year research programme (2016-2022) commissioned by The UK Natural Environment Research Council (NERC) as part of the first wave of a new series of Long Term Science Multi-centre (LTSM) programmes. ACSIS connected research in the physical and chemical components of the atmosphere-hydrosphere-cryosphere nexus within the North Atlantic region and provided an opportunity for NERC scientists from different disciplines to come together and deliver new insights into a region undergoing rapid change in: the ocean and atmosphere temperatures and circulation, in sea ice thickness and extent, and in key atmospheric constituents such as ozone, methane and aerosols (Sutton et al., 2018). The ACSIS team included members of the National Centre for Atmospheric Science (NCAS), Plymouth Marine Laboratory (PML), the National Oceanography Centre (NOC), the British Antarctic Survey (BAS), the National Centre for Earth Observation (NCEO), the Centre for Polar Observation and Modelling (CPOM), and the Met Office.

Deleted:

Deleted: jects

ACSIS was designed to answer key questions about the North Atlantic Climate System:

1) How have changes in natural and anthropogenic emissions and atmospheric circulation combined to shape multi-year trends in North Atlantic atmospheric composition and radiative forcing? 2) How have natural variability and radiative forcing combined to shape multi-year trends in the North Atlantic physical climate system? 3) To what extent are changes in the North Atlantic climate system predictable on multi-year timescales?

Deleted:

In order to answer these questions, ACSIS was arranged into a series of interlinked work packages involving a broad representation of scientists from the different NERC centres involved in ACSIS. These work packages delivered new scientific understanding, delivered through several key synthesis papers (Sutton et al., 2018, Robson et al., 2018, 2020, Hirschi et al., 2020), as well as a wealth of data. [The objectives of ACSIS were:](#)

A) [To provide the UK science community with sustained observations, data syntheses, leading-edge numerical simulations and analysis tools to facilitate world-class research on changes in the North Atlantic climate system and their impacts.](#) B) To provide a quantitative and multivariate description of how the North Atlantic climate system is changing. C) To determine

Deleted:

Deleted: Key

Deleted: the

Deleted: project

Deleted: to

Deleted: P

the primary drivers and processes that are shaping changes in the North Atlantic climate system now and will shape changes in the near future. D) To determine the extent to which future changes in the North Atlantic climate system are predictable.

In this paper we focus on objective (A) of the ACSIS project, which included the creation of new datasets to underpin the ACSIS project and support wider work on the North Atlantic climate system by the UK and international science communities.

In this paper we outline the underpinning datasets generated as part of the ACSIS project, how they can be obtained (guided by the FAIR principles (Wilkinson et al., 2016)), and the motivation for their creation.

1.1 Overview of data holdings

A summary of the datasets that are generated by ACSIS and freely available to the community is given in Table 1. Note that the new data presented in this paper are archived across two platforms: the British Oceanographic Data Centre, <https://www.bodc.ac.uk> (ocean observations) and the Centre for Environmental Data Analysis, <https://www.ceda.ac.uk> (all other data). A schematic map giving an overview of the footprints of all the observational datasets can be found in Fig 1. The three general areas covered are: atmospheric composition covering aircraft and ground station data along with nudged historical atmospheric chemistry/circulation model simulations; ocean observations covering gridded *in situ* temperature and salinity (0-2000m) and 0-1000m heat content; forced historical ocean-ice simulations at eddy permitting and eddy resolving resolutions and standalone Arctic sea ice simulations. In subsequent sections 2, 3 and 4, we describe the individual archived datasets in detail. Several other datasets, previously described in the literature, have been generated by the ACSIS programme including simulations to generate volcanic forcing data for climate models, coupled climate model simulations with a high resolution atmosphere and/or ocean, gridded sea-surface temperature based on in situ ocean observations, and observation based estimates of the Atlantic Meridional Overturning Circulation and Arctic wide sea ice thickness. [We anticipate that all the different types of data used here could be used in synergy and users should take into account the different uncertainties associated with the different datasets. In particular modelled ice, ocean and atmospheric composition are forced by a variety of different atmospheric meteorological data, and this may introduce some further uncertainty into attribution of trends and variability across the different realms.](#) For completeness, and because the new datasets described here will likely be used in conjunction with the already published datasets, we provide a [very](#) brief overview of the latter in Section 5.

Deleted:

Deleted: 4 of Sutton et al. (2018)

Formatted: Font: Italic

Deleted:

Deleted:

Deleted:

Deleted:

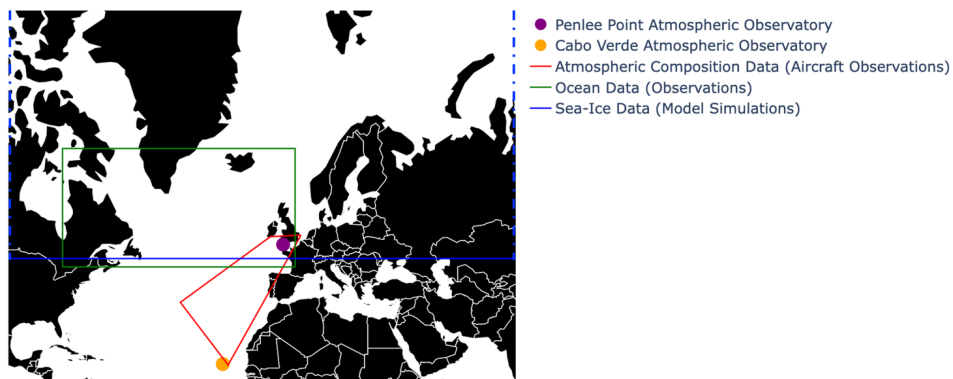


Figure 1. Schematic overview of the footprints of all the observational datasets presented in this paper.

Table 1. Overview of the data described in this paper with links to the sub-sections where the data are described in detail.

Title	Data, weblink, and citation	Accessibility	Subsection
Aircraft missions	Gas and aerosol data collected on board the Facility for Airborne Atmospheric Measurements https://dx.doi.org/10.5285/6285564c34a246fc9ba5ce053d85e5e7 FAAM et al. (2024)	Open access for merged 10s data; registration/login to CEDA required for full temporal resolution.	2.1
Ground based observational atmospheric composition time series	Atmospheric composition, including ozone, methane, carbon monoxide, VOCs and aerosol parameters from the Cape Verde Atmospheric Observatory (CVAO) http://catalogue.ceda.ac.uk/uuid/81693aad69409100b1b9a247b9ae75d5 National Centre for Atmospheric Science et al. (2014) Penlee Point Atmospheric Observatory (PPAO)	CVAO data require registration/login to CEDA. PPAO and PML data	2.2, 2.3

	<p>https://catalogue.ceda.ac.uk/uuid/8f1ff8ea77534e08b03983685990a9b0 Plymouth Marine Laboratory and Yang (2024). Plymouth Marine Laboratory</p> <p>https://catalogue.ceda.ac.uk/uuid/e74491c96ef24df29a9342a3d57b5939 Smyth (2024)</p>	are open access.	
Nudged atmosphere model simulations with atmospheric composition	<p>Simulated atmospheric composition from 1981-2020 with atmospheric circulation nudged to ERA5 reanalysis</p> <p>https://data.ceda.ac.uk/badc/acsis/UKESM1-hindcasts Abraham (2024)</p>	Open access for selected atmospheric composition variables. Requires registration/login on JASMIN and Met Office MASS account for access to comprehensive dataset.	2.4
Ocean circulation and heat content	<p>Objectively interpolated (gridded) ocean temperature and salinity (0-2000m)</p> <p>https://doi.org/10.5285/fe8e524d-7f04-41f3-e053-6c86abc04d51 King (2023)</p> <p>Upper Ocean (0-1000m) heat content time series</p> <p>https://doi.org/10/g6wm Moat et al. (2021a)</p> <p>https://doi.org/10/g8g2 Moat et al. (2021b)</p>	Open access.	3.1,
Ocean-sea ice and standalone sea ice simulations	<p>NEMO-CICE global ocean simulations with default sea ice physics 1°, 1/4° and 1/12° up to 2020</p> <p>https://dx.doi.org/10.5285/119a5d4795c94d2e94f610647640edc0 Megann et al. (2021b)</p> <p>https://dx.doi.org/10.5285/a0708d25b4fc44c5ab1b06e12fef2f2e, Megann et al (2021c)</p>	open access	3.2.2, 4.1

<p>https://dx.doi.org/10.5285/4c545155dfd145a1b02a5d0e577ae37d, Megann et al. (2021d)</p> <p>https://dx.doi.org/10.5285/e02c8424657846468c1ff3a5acd0b1ab Megann et al. (2022a)</p> <p>https://dx.doi.org/10.5285/399b0f762a004657a411a9ea7203493a (Megann et al. (2022b)</p> <p>NEMO-CICE global ocean simulations with improved sea ice physics 1/4^o up to 2020 and standalone Arctic sea ice simulations:</p> <p>http://catalogue.ceda.ac.uk/uuid/770a885a8bc34d51ad71e87ef346d6a8 Megann et al. (2021e)</p>		
---	--	--

Deleted:

2. Composition data sets

The composition of the atmosphere is changing at an unprecedented pace. Changes in the levels of stratospheric ozone, surface ozone and other secondary pollutants are driven by human activities (e.g., Griffiths et al., 2021; Keeble et al., 2020; Turnock et al., 2020). The North Atlantic region has undergone significant growth and decline in air pollution over the last three decades and modelling studies have all shown the significant human health benefits of these more recent reductions (Turnock et al. 2016; Archibald et al., 2017; Daskalakis et al., 2016). But whilst we have a broad understanding of the distribution of key air pollutants and short-lived climate forcers, our understanding of the variability of these species and their trends is hampered across the North Atlantic owing to a paucity of observations. The North Atlantic is frequently impacted by the transport of transboundary pollution from anthropogenic sources and fires (Boylan et al., 2015; Helmig et al., 2015; Kumar et al., 2013), as well as from local natural marine and shipping emissions (e.g., Yang et al., 2016a). High altitude research stations in the Eastern North Atlantic in the Azores (Mt. Pico) and Canary Islands (Izána), coastal observatories on the west coast of Ireland (Mace Head) and in the Cape Verde Islands have provided long term data sets with which to better understand the sources and processes controlling reactive trace gases and aerosols across the North Atlantic.

Deleted:

In ACSIS a series of work packages were conducted to a) further our understanding of the distribution and variability of key trace gases and aerosols using aircraft campaigns and long-term measurements, b) understand the processes controlling these and c) improve model simulations, which can be used to forecast the future evolution of these species. In the following sections we outline the data that were generated to support these objectives.

2.1 Aircraft campaigns in the North Atlantic

[During ACSIS approximately biannual gas and aerosol composition measurements on aircraft missions from the UK to the Azores were made, focusing on obtaining vertical context for composition, to complement surface observations and provide linkage with satellite data.](#)

[Measurements were collected using the UK's Atmospheric Research Aircraft \(ARA\). The ARA is a BAe-146-301 which has been in service since 2004 and is managed by the Facility for Airborne Atmospheric Measurements \(FAAM\), an airborne laboratory funded by the UK government. The FAAM aircraft is capable of carrying a 4-tonne instrument load and can operate at altitudes between 50 and 30000 ft \(15–9140 m\), allowing the study of processes in the troposphere and boundary layer. ARA missions as part of ACSIS provide the longest record of composition change in the lower free troposphere over the North Atlantic \(Sutton et al., 2018\) and further complemented historic research flights conducted with the ARA in the region \(e.g., Parrington et al., 2012; Reeves et al., 2002\) and more recent flights by other platforms \(e.g., ATom \(Wofsy et al., 2018\), NAAMES \(e.g., Behrenfeld et al., 2019; Sinclair et al., 2020\) and ACE-ENA \(Zawadowicz et al., 2021\).](#)

2.1.1 Campaign Flights

[A series of \(daytime\) research flights were carried out across the North Atlantic Ocean from February 2017 – May 2022. Fig. 2 shows the location of the ACSIS flight tracks, coloured by campaign number. There were a total of 45 flights as part of the ACSIS campaign, comprising close to 200 hours of measurement data. Measurements were made from approximately 50 m over the sea surface to 9140 m. ACSIS 1, 2, 4, 5 and 7 were predominantly based out of the Azores, whilst flights for ACSIS 3 were based out of Cork, Ireland and ACSIS 6 flights based out of Cape Verde.](#)

[Also shown in Fig. 2 are part of the flight tracks for the NASA Atmospheric Tomography Mission \(ATom\) mission. The ATom campaigns aimed to improve the representation of reactive gases and short-lived climate forcers in global atmospheric chemistry and climate models by measuring atmospheric composition along a global circuit flight track \(Prather et al., 2017\). Four ATom campaigns occurred between August 2016 and May 2018. The ATom data set is complementary to that collected during the ACSIS flight campaigns; ATom flights provided a broad overview on a global scale, whereas ACSIS flights intensively measured the North Atlantic region. ACSIS-1 overlapped with ATom2 and ACSIS-2 overlapped with ATom3.](#)

Deleted: ure

Deleted: 1

Deleted: 7600

Deleted: 1

Deleted: A series of (daytime) research flights were carried out across the North Atlantic Ocean from February 2017 – May 2022. Measurements were collected using the UK's Atmospheric Research Aircraft (ARA). The ARA is a BAe-146-301 which has been in service since 2004 and is managed by the Facility for Airborne Atmospheric Measurements (FAAM), an airborne laboratory funded by the UK government. The FAAM aircraft is capable of carrying a 4-tonne instrument load and can operate at altitudes between 50 and 30000 ft (15–9140 m), allowing the study of processes in the troposphere and boundary layer. ARA missions as part of ACSIS provide the longest record of composition change in the lower free troposphere over the North Atlantic (Sutton et al., 2018) and further complemented historic research flights conducted with the ARA in the region (e.g., Parrington et al., 2012; Reeves et al., 2002) and more recent flights by other platforms (e.g., ATom (Wofsy et al., 2018), NAAMES (e.g., Behrenfeld et al., 2019; Sinclair et al., 2020) and ACE-ENA (Zawadowicz et al., 2021)). A wide range of instrumentation are fitted on the ARA, including measurements of key meteorological parameters such as temperature, humidity, wind speed and direction as well as a range of in situ trace gas measurements including carbon monoxide (CO), ozone (O₃), oxides of nitrogen (NO_x=NO+NO₂), and the greenhouse gases carbon dioxide (CO₂) and methane (CH₄). Table 2 below summarises the measurement techniques and uncertainties onboard the ARA that were used during ACSIS flights. ¶

¶ **Table 2.** A summary of atmospheric chemistry instrumentation used during the ACSIS flights onboard the FAAM BAe-146-301 Atmospheric Research Aircraft. ¶
Measurement ¶ [1]

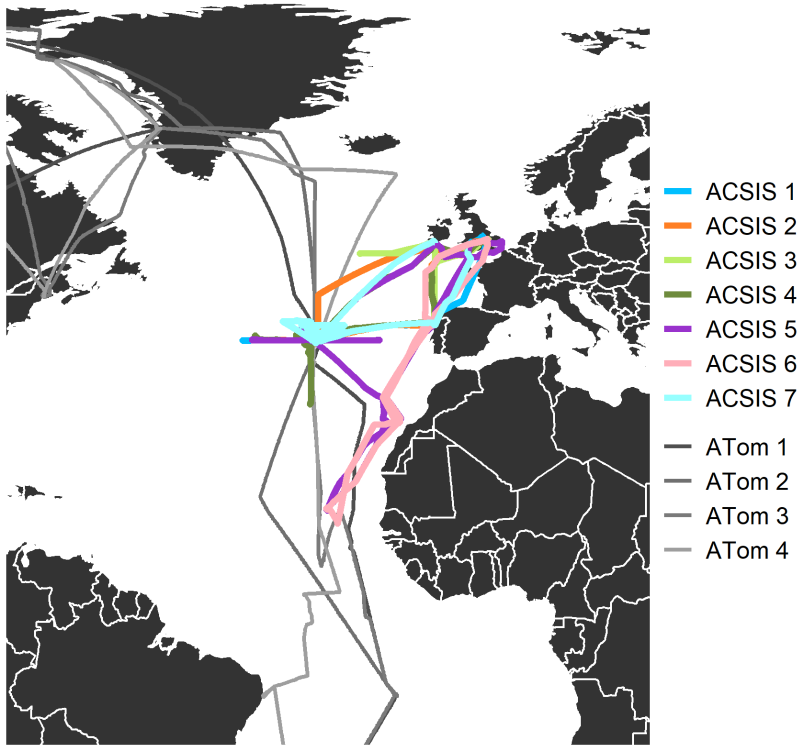


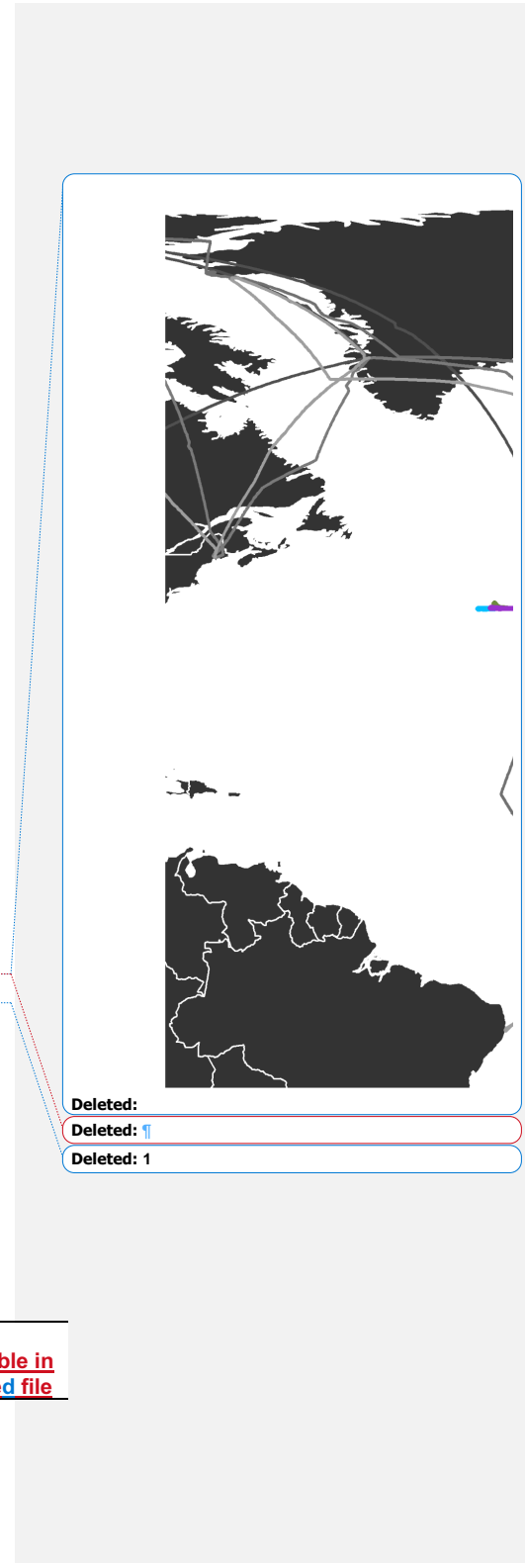
Figure 2. A map of flight tracks for the seven ACSIS ARA campaigns. Part of the NASA ATom flight campaign flight tracks are shown in grey for comparison.

2.1.2 Instrumentation

A wide range of instrumentation are fitted on the ARA, including measurements of key meteorological parameters such as temperature, humidity, wind speed and direction as well as a range of in situ trace gas measurements including carbon monoxide (CO), ozone (O₃), oxides of nitrogen (NO_x=NO+NO₂), and the greenhouse gases carbon dioxide (CO₂) and methane (CH₄). Table 2 below summarises the measurement techniques, uncertainties and limit of detection (i.e. precision 3σ) onboard the ARA that were used during ACSIS flights.

Table 2. A summary of atmospheric chemistry instrumentation used during the ACSIS flights onboard the FAAM BAe-146-301 Atmospheric Research Aircraft.

<u>Measurement</u>	<u>Instrumentation</u>	<u>Time resolution</u>	<u>Precision</u> 3σ	<u>Uncertainty</u>	<u>Timescale</u>	<u>Data available in merged file</u>
--------------------	------------------------	------------------------	------------------------	--------------------	------------------	--------------------------------------



<u>O₃</u>	<u>Thermo 49i ozone photometer</u>	<u>4 sec</u>	<u>6 ppb</u>	<u>3 ppb / 3%</u>	<u>2017-2021</u>	<u>X</u>
<u>O₃</u>	<u>2BTechnologies Model 205 ozone photometer</u>	<u>2 sec</u>	<u>4 nmol mol⁻¹</u>	<u>5 ppb / 3% for O₃ ≥ 100 nmol mol⁻¹</u>	<u>2022-present</u>	<u>X</u>
<u>CO</u>	<u>AeroLaser AL5002 (VUV RF)</u>	<u>1 sec</u>	<u>6 ppb</u>	<u>2 ppb</u>	<u>2005-2019</u>	<u>X</u>
<u>CO₂</u>	<u>Los Gatos Research FGGA (OA-ICOS)</u>	<u>1 sec</u>	<u>1.5 ppm</u>	<u>0.5 ppm</u>	<u>2011-present</u>	<u>X</u>
<u>CH₄</u>	<u>Los Gatos Research FGGA (OA-ICOS)</u>	<u>1 sec</u>	<u>6 ppb</u>	<u>3 ppb</u>	<u>2011-present</u>	<u>X</u>
<u>NO</u>	<u>Chemiluminescence Air Quality Design Inc</u>	<u>10 sec</u>	<u>10 ppt</u>	<u>24%</u>	<u>2009-2019</u>	<u>X</u>
<u>NO₂</u>	<u>Chemiluminescence Air Quality Design Inc</u>	<u>10 sec</u>	<u>13 ppt</u>	<u>41%</u>	<u>2009-2019</u>	<u>X</u>
<u>NO</u>	<u>Chemiluminescence Air Quality Design Inc (upgraded)</u>	<u>0.1 sec</u>	<u>30 ppt</u>	<u>24%</u>	<u>2019-present</u>	<u>X</u>
<u>NO₂</u>	<u>Chemiluminescence Air Quality Design Inc (upgraded)</u>	<u>0.1 sec</u>	<u>60 ppt</u>	<u>41%</u>	<u>2019-present</u>	<u>X</u>
<u>SO₂</u>	<u>University of York laser-induced fluorescence sulfur dioxide detector (LIF-SO₂)</u>	<u>1 sec</u>	<u>225 ppt</u>	<u>15 %</u>	<u>2022-present</u>	<u>X</u>
<u>Solar Actinic flux</u>	<u>Ocean Optics QE Pro, up and downward facing UV-vis (280-700 nm) spectrometers</u>	<u>1 sec</u>	<u>TBC</u>	<u>5 %</u>	<u>2019-present</u>	<u>X</u>
<u>HCHO</u>	<u>LIF pulsed 353.370 nm spectrometer, Thermo Scientific Model TFL 3000 Novawave</u>	<u>1 sec</u>	<u>n/a</u>	<u>n/a</u>	<u>2019-present</u>	

VOCs	Whole Air Samples and offline analysis by GC-FID or GC-MS	n/a			2005-present
Other gases	University of Manchester High Resolution-Time of Flight-Chemical Ionisation Mass Spectrometer (ToF-CIMS)	0.25 sec		10-20%	2019-present
HONO	ToF-CIMS	0.25 sec	n/a	20%	
HCN	ToF-CIMS	0.25 sec		30%	X
BrO	ToF-CIMS	0.25 sec	n/a	40%	
BrCl	ToF-CIMS	0.25 sec	n/a	40%	
CINO ₂	ToF-CIMS	0.25 sec		30%	X
Cl ₂	ToF-CIMS	0.25 sec	n/a	20%	
ClO	ToF-CIMS	0.25 sec	n/a	40%	
HPMTF [§]	ToF-CIMS	0.25 sec	n/a	n/a	
Urea	ToF-CIMS	0.25 sec	30 ppt	25%	X
Submicron Aerosol Compositio	University of Manchester Aerosol Mass Spectrometer (AMS)				2019-present (excl. 2020)
η Organic	AMS	8-15 sec	0.03 μg/m ³	38%	X
SO ₄	AMS	8-15 sec	0.03 μg/m ³	36%	X
NH ₄	AMS	8-15 sec	0.03 μg/m ³	34%	X
NO ₃	AMS	8-15 sec	0.03 μg/m ³	34%	X
nss-Cl	AMS	8-15 sec	0.03 μg/m ³	n/a	X

[§]Hydroperoxy methyl thioformate.

2.1.3 Vertical Distribution of Pollutants

Data collected during flights from all seven ACSIS campaigns have been analysed together to give insights into the spatial and vertical characteristics of atmospheric composition over the North Atlantic Ocean. Data from all seven campaigns have been combined and grouped into 1000 m altitude bins. Fig. 3 shows the vertical distribution of O₃, CO, CO₂, CH₄, NO and NO₂. Table 3 summarises the flights and times that were used in this bulk analysis.

Deleted: 7

Deleted: ure

Deleted: 2

Moved down [1]: ¶

Table 3. Summary of flights used in bulk analysis of atmospheric composition data. ¶
Campaign

Deleted: Also shown in Fig. 1 are part of the flight tracks for the NASA Atmospheric Tomography Mission (ATom) mission. The ATom campaigns aimed to improve the representation of reactive gases and short-lived climate forcers in global atmospheric chemistry and climate models by measuring atmospheric composition along a global circuit flight track (Prather et al., 2017). Four ATom campaigns occurred between August 2016 and May 2018. The ATom data set is complementary to that collected during the ACSIS flight campaigns; ATom flights provided a broad overview on a global scale, whereas ACSIS flights intensively measured the North Atlantic region. ACSIS-1 overlapped with ATom2 and ACSIS-2 overlapped with ATom3. ¶

2.1.1 Bulk Analysis of Data ¶

Data collected during flights from all 7 ACSIS campaigns have been analysed together to give insights into the spatial and vertical characteristics of atmospheric composition over the North Atlantic Ocean. Table 3 summarises the flights and times that were used in this bulk analysis. ¶

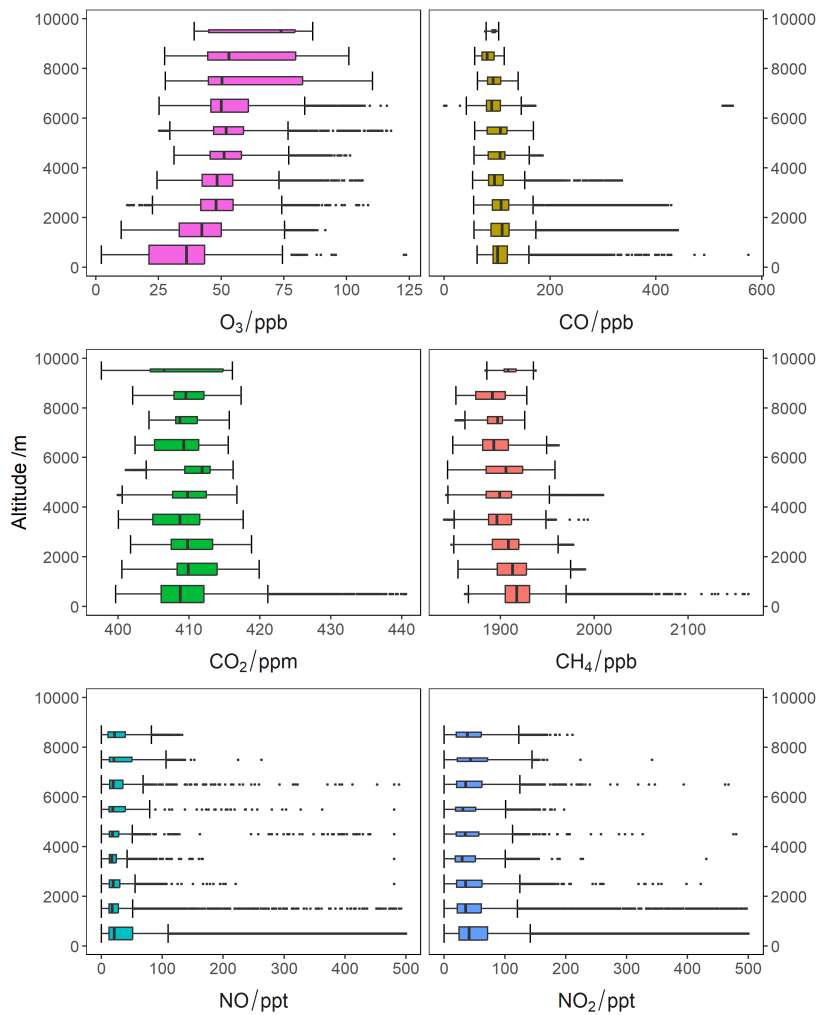


Figure 3. Box plots showing the vertical distribution of O₃, CO, CO₂, CH₄, NO and NO₂ for all seven ACSIS campaigns. The vertical line in the centre of each box represents the median value with the edges of the boxes showing the 25th and 75th percentiles. The bars extending from the box show the minimum and maximum values no more than 1.5 times the interquartile range. The height of the box is proportional to the number of observations within each altitude bin, with taller boxes corresponding to a higher number of observations. Note that sporadic high mixing ratios of CO, NO and NO₂ at low altitudes, likely due to local pollution sources, have been filtered so that the bulk of the data is clearly shown. Cut off values of 600 ppbv for CO and

Deleted: 1

500 pptv for NO and NO₂ were used. The NO_x instrument has a ceiling of ~8200 m so there is no data for the 9000 – 10000 m bin.

Table 3. Summary of flights used in bulk analysis of atmospheric composition data.

Campaign	Flight Numbers	Date Range	Comments
ACSIS 1	<u>B996, B997, B998, B999, C001, C002</u>	<u>13/02/2017 – 16/02/2017</u>	
ACSIS 2	<u>C066, C067, C068, C070, C071</u>	<u>19/10/2017 – 23/10/2017</u>	
ACSIS 3	<u>C103, C105, C106</u>	<u>14/05/2018 – 17/05/2018</u>	<u>No greenhouse gas data available due to the FGGA fault.</u>
ACSIS 4	<u>C139, C140, C141, C142, C143, C144, C145</u>	<u>19/02/2019 – 22/02/2019</u>	<u>No VOC data on CEDA</u>
ACSIS 5	<u>C199, C200, C201, C202, C203, C204, C205, C210, C211, C212</u>	<u>13/08/2019 – 22/08/2019</u>	
ACSIS 6	<u>C215, C216, C217, C226, C227, C228, C229</u>	<u>04/02/2020 – 14/02/2020</u>	
ACSIS 7	<u>C288, C289, C290, C291, C292, C293, C294</u>	<u>03/05/2022 – 09/05/2022</u>	

Moved (insertion) [1]

2.1.4 Data archive

To accompany this paper a 10 second averaged merged file has been created for each flight listed in Table 3 (<https://dx.doi.org/10.5285/6285564c34a246fc9ba5ce053d85e5e7>, Facility for Airborne Atmospheric Measurements et al., 2024). The merged files are open access and designed to be a tool for an initial exploration of the data and to highlight the breadth of the atmospheric composition data collected during the ACSIS programme. However, for further analysis the original frequency data should be used and details of where these files can be found is included in the header information of the merged files. The merged files are in ascii format and consist of a short explanatory paragraph followed by a list of variables and finally the data arranged as columns, with one variable per column with rows corresponding to the values at each 10s time interval.

Formatted: Font: Not Bold, Not Italic

Deleted: ¶

2.2 Cape Verde Atmospheric Observatory (CVAO)

ACSIS supported composition measurements at Cape Verde from 2016 to 2021 in order to deliver: quantitative analyses of composition variability and its relationship to other climate parameters; trend analyses on the long-term surface-based data sets; understanding of how these link to patterns identified in the aircraft and satellite observations.

The Global GAW Cape Verde Atmospheric Observatory is situated in Calhau on the island of Sao Vicente in the Republic of Cabo Verde (16.848°N, 24.871°W, 10m asl,

<https://amof.ac.uk/observatory/cape-verde-atmospheric-observatory-cvao/>). Measurements were started in October 2006 to further our understanding of atmospheric chemistry within the tropical marine boundary layer and North Atlantic region. The site receives air from a wide variety of sources with 10-day back trajectories reaching to North America, Europe and sub-Saharan Africa (see Carpenter et al. (2010) for details). Long term high frequency measurements allow investigation into the trends of climate gases such as CO₂ and CH₄ whilst measurements of pollutants from the continents such as hydrocarbons and nitrogen oxides provide better constraints of global emission changes and their effect on the long-term background of the North Atlantic (e.g., Helmig et al., 2016). The Observatory regularly hosts field campaigns which focus on process studies such as sea-surface interactions and the role of aerosols in atmospheric chemistry (Read et al., 2008, McFiggans et al., 2009, Lawler et al., 2011, Van Pinxteren et al., 2020).

2.2.1 Time series of meteorological parameters and chemical composition

Table 4 provides a summary of the chemical species recorded at the CVAO and Figs. 4 and 5 show time series of meteorological parameters and concentrations of chemical species. During ACSIS these time series were used to estimate trends, particularly in ozone, carbon monoxide, methane and NO_x. Here we make some general observations concerning the time series of these four species (Figure 4). Ozone concentrations at the CVAO show seasonal variability with highest concentrations in spring and lowest in summer, consistent with its role as a secondary pollutant. In summer, the site occasionally receives air from the southern hemisphere during the early stages of the Atlantic cyclonic activity, which leads to very low concentrations of ozone (<10 ppb) observed along with episodes of intense precipitation. Carbon monoxide is a primary pollutant emitted from anthropogenic sources and from biomass burning. Since 2008 CO has been decreasing at CVAO. Global methane concentrations have increased substantially over the last 10 years, attributed to increased primary emissions of hydrocarbons and increased emissions from wetlands due to increasing temperatures (Jackson et al. 2020, Thompson et al., 2018). At CVAO methane has been increasing steadily. Concerning NO_x, in extremely clean air containing low levels of CO and VOCs, Andersen et al. (2022) showed good agreement between NO₂ levels observed at the CVAO and those derived from the photostationary state (PSS), utilising measured NO, O₃, and jNO₂ and photo-chemical box model predictions of peroxy radicals. However, in clean air containing small amounts of aged pollution, as typically encountered in winter, higher levels of NO₂ were observed than inferred from the PSS, implying underestimation of peroxy radicals or unattributed NO₂ measurement artefacts.

Table 4. Summary of atmospheric data recorded at CVAO.

Measurement	Instrumentation	Time resolution	Precision (1hr)	Timescale
O ₃	Thermo 49i ozone monitor	10 sec	0.5 ppb	2006-present
CO	Aerolaser AL5001/ Picarro G4201	4 sec	1 ppb	2008-present

Deleted:

Deleted: Recent work has provided evidence for the rapid photolysis of nitrate aerosol as an important source of HONO and NO₂ to the marine troposphere (Andersen et al., 2021). Andersen et al. (2023) confirmed the ubiquity of this so-called "renoxification" source of HONO and NO_x in the remote Atlantic troposphere using HONO observations at the CVAO and from aircraft in the surrounding remote Atlantic troposphere and showed evidence for renoxification occurring on marine and mixed marine/dust and biomass burning aerosols with an efficiency that increased with relative humidity and decreased with the concentration of nitrate.

Formatted: Font: Bold

Formatted: Font: Not Bold, Not Italic

Formatted: Subscript

Formatted: Subscript

Formatted: Subscript

Formatted: Subscript

Commented [EM1]: They are happy for these sections to be removed if Ming has done the same for Penlee

Formatted: Font: 10 pt, Bold

NO	Chemiluminescence instrument Air Quality Design Inc. (AQD), USA	5 min	1.4 ppt	2006-present
NO ₂	Chemiluminescence instrument Air Quality Design Inc. (AQD), USA	5 min	4.4 ppt	2017-present
VOCs	GC-FID	1 hour		2006-present
OVOCs	GC-FID	1 hour		2014-present
Short-lived halocarbons	GC-MS-TOF	1 hour		2014-present
CFCs/HCFCS	GC-MS-TOF	1 hour		2022-present
DMS	GC-FID	1 hour		2012-present
Photolysis rates	Spectral radiometer	1 min		2016-present
CO ₂	Picarro G4201	4 sec	10 ppb	2012-present
CH ₄	Picarro G4201	4 sec	0.3 ppb	2012-present
SO ₂	Thermo 43i HL	5 sec		2019-present
Total Gaseous Mercury	Tekran	1 min		2014-2019

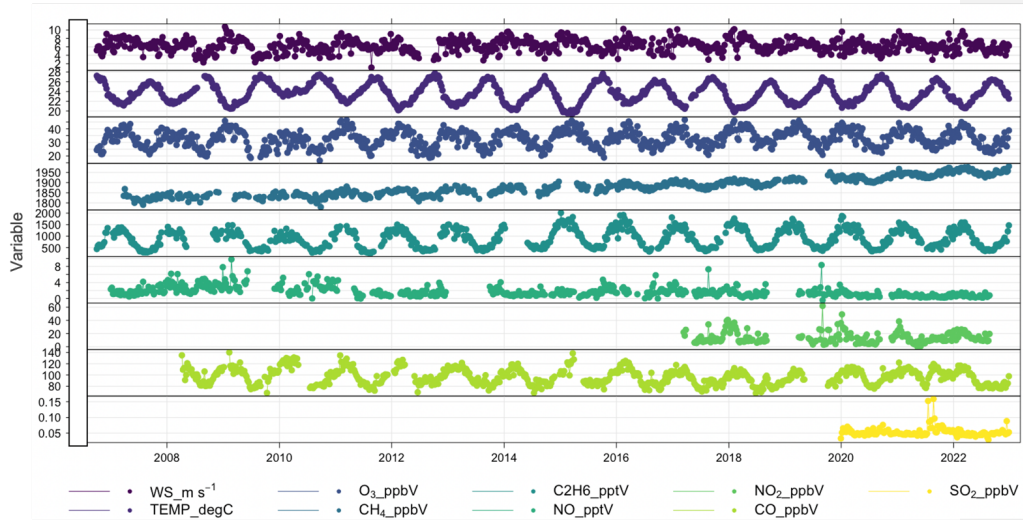


Figure 4. Time series of weekly averaged Cape Verde data showing a range of species and meteorological parameters measured from 7.5m between 2006-2022. From top: wind speed, ambient temperature, ozone, methane, ethane, nitric oxide, nitrogen dioxide, carbon monoxide and sulphur dioxide.

Deleted: 3

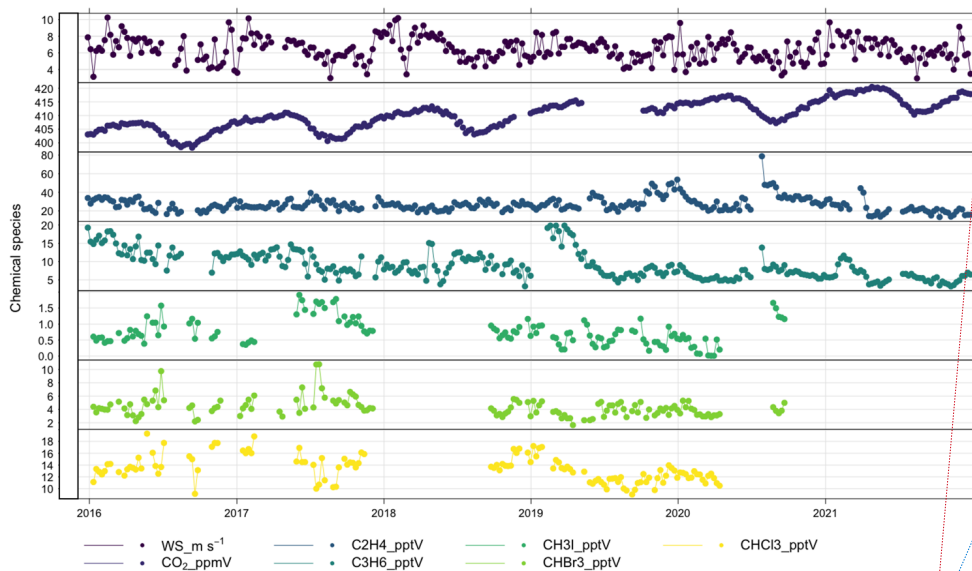
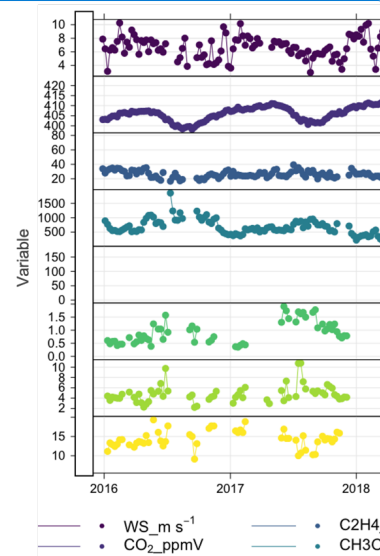


Figure 5. Time series of weekly averaged Cape Verde data showing a range of species and meteorological parameters measured from 7.5m between 2016-2021. From top: wind speed, carbon dioxide, ethene, propene, methyl iodide, bromoform and chloroform.

2.2.2 Data archive

Cape Verde data collected under the auspices of ACSIS is available from CEDA: <http://catalogue.ceda.ac.uk/uuid/81693aad69409100b1b9a247b9ae75d5> (National Centre for Atmospheric Science et al. (2014)). Note that there are a number of subdirectories, some of which are not relevant to the data described in this paper. The relevant subdirectories are labelled with the variable or variable group and the time period (e.g. Cape Verde Atmospheric Observatory: Ozone measurements (2006 onwards)). The data format is ASCII, consisting of a header explaining the variables listed followed by the data in columnar format (one column per variable), with the data values in rows appearing in chronological order. We note that specific Cape Verde data is also archived at the World Data Centre for Greenhouse Gases, <https://gaw.kishou.go.jp> (CO₂, CH₄ and CO) and at EBAS, <https://ebas.nilu.no> (VOCs, NO_x, SO₂ and halocarbons).

Deleted: Time series of Cape Verde data showing a range of the species and meteorological parameters measured..



Deleted:

Deleted: 4

Formatted: Line spacing: 1.5 lines

Deleted: Time series of weekly averaged Cape Verde data showing a range of species and meteorological parameters measured from 7.5m between 2016-2022. From top: wind speed, carbon dioxide, ethene, methanol, dimethyl sulphide, methyl iodide, bromoform and chloroform.

Deleted: ¶

Deleted: 5

... [2]

2.3 Penlee Point Atmospheric Observatory

[As with CVAO, ACSIS also supported atmospheric composition observations at Penlee Point, UK. Situated on the eastern edge of the North Atlantic, the Penlee Point Atmospheric Observatory \(PPAO; 50° 19.08' N, 4° 11.35' W; <https://www.westernchannelobservatory.org.uk/penlee/>\) was established by the Plymouth Marine Laboratory \(PML\) in 2014 on the southwest coast of the United Kingdom. PPAO is a few tens of metres away from the water edge and about 11 m above mean sea level. The site is exposed to marine air over a very wide sector \(wind directions of ~110-260°\). Typical southwesterly winds tend to bring relatively clean background air coming off the North Atlantic, with little terrestrial influence. Winds from the southeast are often contaminated by exhaust plumes from passing ships, while winds from the north are influenced by terrestrial emissions.](#)

[In close proximity to the Western Channel Observatory marine sampling stations, high frequency observations at PPAO enable both long-term monitoring of trends and process-based studies of atmosphere-ocean interactions. Current/recent work has assessed trace gas burdens and air-sea fluxes including greenhouse gases \(Yang et al. 2016b, 2016c, 2019a\), volatile organic carbon \(Phillips et al., 2021\), sulfur- \(Yang et al., 2016c\), halogen- \(Sommariva et al., 2018\), and nitrogen-containing gases \(ongoing\). Further works include aerosol composition and fluxes, with particular foci on ship emissions \(ongoing as a part of the ACRUISE project\), sea spray production \(Yang et al., 2019b\), macro/micro nutrient deposition \(White et al., 2021\), and reaction between atmospheric ozone and the sea surface microlayer \(Loades et al., 2020\).](#)

Continuous observations most relevant to ACSIS include ground-based ozone and methane from PPAO as well as column aerosols from the rooftop of PML (10 km north/northeast of PPAO). These measurements are detailed in Table 5.

Table 5. Overview of the measurements made at PPAO.

Measurement	Instrumentation	Time resolution	Accuracy	Timescale
O ₃	(a) 2B 205 ozone monitor; (b) Thermo 49i ozone monitor	10 sec	≤1 ppb	(a) May 2014 – Sept 2018 (b) Sept 2018 – present
CH ₄	(a) Picarro G2311-f; (b) Los Gatos Research Fast Greenhouse Gas Analyzer	0.1 sec until Aug 2016; 1 sec since Aug 2016	≤ 3 ppb	(a) May 2014 – Sept 2015 (b) Sept 2015 – present
Aerosols	POM sunphotometer	10 min (when clear sky and during the day)	≤0.01 at 550 nm	2001 – present

2.3.1 Ozone

Deleted: Penlee Point Atmospheric Observatory (PPAO; 50° 19.08' N, 4° 11.35' W; <https://www.westernchannelobservatory.org.uk/penlee/>) was established by the Plymouth Marine Laboratory (PML) in 2014 on the southwest coast of the United Kingdom. At the western mouth of the Plymouth Sound and near the tip of the Rame Peninsula, PPAO is a few tens of metres away from the water edge and about 11 m above mean sea level. The site is exposed to marine air over a very wide sector (wind directions of 110-240°). Typical south-westerly winds tend to bring relatively clean background air coming off the North Atlantic. Winds from the southeast are often contaminated by exhaust plumes from passing ships, while winds from the north are influenced by terrestrial emissions. ¶
In close proximity to the Western Channel Observatory marine sampling stations, high frequency observations at PPAO enable both long-term and process-based studies of atmosphere-ocean interactions. Current/recent work has assessed trace gas burdens and air-sea fluxes including greenhouse gases (Yang et al. 2016b, 2016c, 2019a), volatile organic carbon (Phillips et al., 2021), sulfur- (Yang et al., 2016c), halogen- (Sommariva et al., 2018), and nitrogen-containing gases (ongoing). Further works include aerosol composition and fluxes, with particular foci on ship emissions (ongoing as a part of the ACRUISE project), sea spray production (Yang et al., 2019b), macro/micro nutrient deposition (White et al., 2021), and reaction between atmospheric ozone and the sea surface microlayer (Loades et al., 2020)¶

Due to the short lifetime of O_3 , it is sensitive to local sources/sinks and heterogeneities associated with a coastal environment. This presents a good opportunity to compare two different methods of identifying the southwest (i.e. Atlantic) wind sector: 1) by airmass dispersion history (NAME (Numerical Atmospheric-dispersion Modelling Environment), see e.g. Yang and Fleming, 2019), and 2) by local wind direction. Data from the first two years of observations (May 2014 to Apr 2016, when NAME model output was available) show that defining the PPAO open ocean sector either by local wind direction (210 to 260°) or by airmass history (>80% in the Atlantic Ocean region over the last 5 days) yield fairly comparable results, with a mean difference of about 1.5 ppb. In subsequent analyses, we define the southwest (Atlantic) wind sector by local wind direction only as the NAME modelling for PPAO is unavailable after Mar 2017.

2.3.2 Methane

As shown in Figure 6, the overall mean CH_4 mixing ratio is about 0.02-0.03 ppm higher than the mean CH_4 from the southwest wind sector (here defined as wind direction between 210 and 260 degrees). This illustrates the importance in considering wind sectors in interpretation of coastal observations. The long-term trends in CH_4 mixing ratio are similar with or without the wind sector consideration, and are in line with observations made globally (e.g., Nisbet et al. 2019).

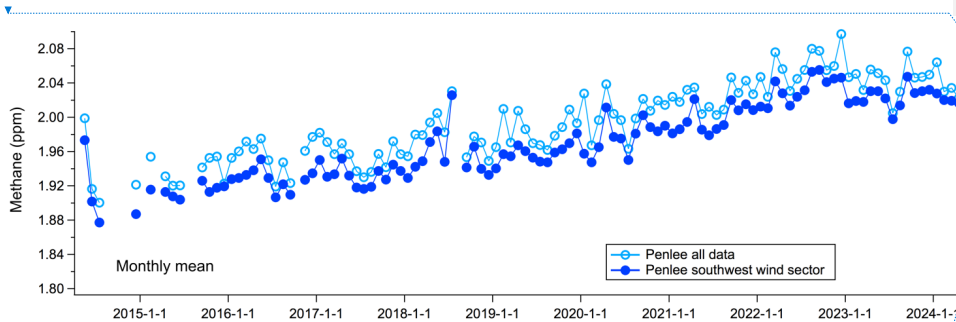


Figure 6: Long-term measurements of methane from PPAO showing a strong long-term increase.

Methane shows a mean seasonal amplitude of ~ 0.03 ppm (relative difference of $\sim 1.5\%$). The summer minimum is most likely due to an increased sink of methane by the OH radical. These data suggest no significant deviation from the long-term trend over the last few years (2019-2022), when it has been postulated that the COVID lockdowns changed the atmospheric oxidising capacity and so the OH sink (e.g., Stevenson et al., 2022).

2.3.3 Aerosols from sunphotometers

Long-term aerosol measurements (starting from 2001) have been made from the rooftop of PML (50.3661° N, 4.1482° W, about 10 km NNE of Penlee Point). The retrieved, cloud-filtered data are averaged to monthly intervals as shown in Figure 7a. Overall there is no obvious long term

Formatted: Justified, Space Before: 14 pt, After: 14 pt, Border: Top: (No border), Bottom: (No border), Left: (No border), Right: (No border), Between : (No border)

Moved (insertion) [2]

Deleted: open ocean

Deleted: model

Deleted: ¶

We first examine the ground-based O_3 observation, focusing especially on variability within the open ocean (e.g. Atlantic) wind sector. Here we limit our analysis to

Deleted:)

Deleted: airmass dispersion modelling (NAME)

Moved up [2]: This presents a good opportunity to compare two different methods of identifying the open ocean wind sector: 1) by airmass history, and 2) by local wind direction.

Deleted: to assess the airmass history (see Yang and Fleming, 2019). Due to its short lifetime, we expect O_3 to be more sensitive than CH_4 to local sources/sinks and heterogeneities associated with a coastal environment. This presents a good opportunity to compare two different me... [3]

Deleted: open ocean

Deleted: ¶

¶

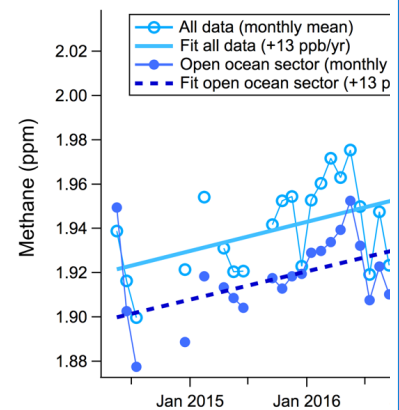
... [4]

Deleted: 5

Deleted: 4

Deleted: open-ocean

Deleted: The long-term increase in the dry-air mixing ratio of CH_4 (Figure 5) is significant, 13 ppb/yr, and in line with ... [5]



Deleted:

Deleted: 4

Deleted: 5

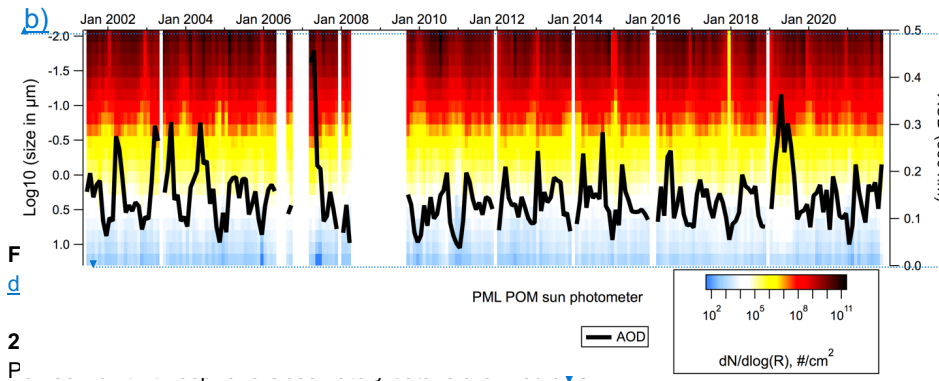
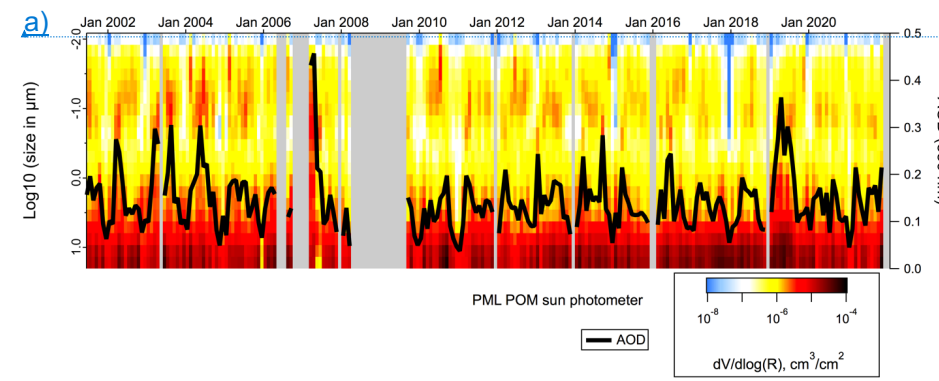
Deleted: Figure 5: Long-term measurements of methane made at PPAO highlighting the strong increase in methane. ¶

Commented [MX4]: Remove?

Deleted: 6

trend in Aerosol Optical Depth (AOD) at this site, in contrast to many other locations in Western Europe that tend to show a gradual reduction. This may be because of the predominance of sea spray aerosols at this location (Yang et al. 2020).

The inferred size distributions are also shown (Fig. 7b). The volume distribution ($dV/d\log(R)$) is dominated by super-micron aerosols, while the number distribution ($dN/d\log(R)$) is dominated by sub-micron aerosols. There appears to be a gradual reduction in springtime aerosol maximum at around 100 nm radius from 2010 to 2021, which could be related to reduced terrestrial or ship anthropogenic emissions (e.g. due to air quality related regulations).



F
d
2
P

<https://catalogue.ceda.ac.uk/uuid/8f1ff8ea77534e08b03983685990a9b0> (Plymouth Marine Laboratory and Yang (2024)). Data from the PML sun photometer can be found at <https://dx.doi.org/10.5285/e74491c96ef24df29a9342a3d57b5939> (Smyth (2024)) The data format is ASCII, consisting of a header explaining the variables listed followed by the data in columnar format (one column per variable), with the data values in rows appearing in chronological order.

Deleted: 6

Formatted: Font: 14 pt

Formatted: Font: 14 pt

Deleted: 6

Deleted: the

Deleted:

2.4 Atmospheric composition modelling with UKESM1

[To complement the observational data, ACSIS performed climate model experiments with full atmospheric chemistry included. The experimental design for these simulations was focussed around providing simulations and output that could support observational campaigns and allowed for a detailed analysis of model transport and composition processes. As well as all the chemical and aerosol fields, fluxes through all chemical reactions and deposition processes were output as monthly means. Model restart files were also saved to allow for re-running short sections with an increased \(and higher frequency\) output request to compare against flight campaigns. Updates to the experiments were made throughout the project, incorporating bugfixes and model improvements. The simulations performed are listed in Table 6.](#)

Model integrations were performed using a nudged (Telford et al., 2008) configuration of the UKESM1 Earth system model (Sellar et al., 2019) at Unified Model version 11.5. For nudged model integrations, the horizontal wind fields and potential temperature are relaxed to either the ERA-Interim (Dee et al., 2011) or ERA-5 (Hersbach et al., 2020) datasets using an e-folding relaxation timescale of 6 h. Sea-surface temperatures and sea-ice fields were prescribed from the Reynolds dataset (Reynolds et al., 2002). [UKESM simulations were performed using the StratTrop chemical scheme which simulates the O_x, HO_x and NO_x chemical cycles and the oxidation of carbon monoxide, ethane, propane, and isoprene in addition to chlorine and bromine chemistry, including heterogeneous processes on polar stratospheric clouds \(PSCs\) and liquid sulfate aerosols \(SAs\). The two-moment GLOMAP-mode aerosol scheme from UKCA \(Mulcahy et al., 2020\), is used to simulate sulfate and secondary organic aerosol \(SOA\) formation and is driven by prescribed oxidant fields. For further details on UKESM chemistry and aerosols scheme the reader is referred to Archibald et al. \(2020\).](#) Simulations were performed from 1981 to 2014 using CMIP historical forcings (labelled as HIST) and continued until 2019 (ERA-Interim) or 2020 (ERA-5) using SSP3-7.0 forcings (labelled as SCEN) as per the AerChemMIP experiment definition (Collins et al., 2017) (see Table 6) for details.

In order to identify the impact of transport on modelled tropospheric ozone in the North Atlantic, the following diagnostic tracers were also defined:

- 4 different stratospheric ozone tracers (O3_s) were added. These are constrained in the stratosphere and evolve freely in the troposphere where they follow equivalent loss processes to the prognostic ozone field simulated by the model. The 4 O3_s tracers are described below:
 1. Stratospheric concentrations are set to the prognostic ozone field above a model diagnosed tropopause defined by the 2PV+380K surface.
 2. Stratospheric concentrations are fixed at 1 ppmv above a model diagnosed tropopause defined by the 2PV+380K surface.
 3. Stratospheric concentrations are set to the prognostic ozone field above a model diagnosed tropopause defined by the WMO tropopause definition.

Deleted: Atmospheric composition was simulated using the UKCA chemistry module, applying the stratosphere-troposphere chemical mechanism of Archibald et al. (2020) with the 2-moment prognostic aerosol scheme as described in Mulcahy et al. (2020)

Deleted:

Deleted:

4. Stratospheric concentrations are fixed at 1 ppmv above a model diagnosed tropopause defined by the WMO tropopause definition.

Tracers 1 and 3 are similar to the O_3_s tracers used in the CCMI experiments (Abalos et al., 2020) and represent tropospheric ozone originating from the stratosphere, while tracers 2 and 4 (also referred to as constant O_3_s tracers or O_{3s-c}) give a complementary measure of downward transport from the stratosphere that is not affected by stratospheric ozone geographical distribution or trends (Russo et al., 2023). An example of tracer 1 tropospheric column and its seasonal variation is given in Fig. 8a-d.

- 30 regionally emitted tracers were included to diagnose long range transport into the North Atlantic region. These have either a lifetime of 5 or 30 days and emission regions are sketched in Figure 8e.

Deleted: ure

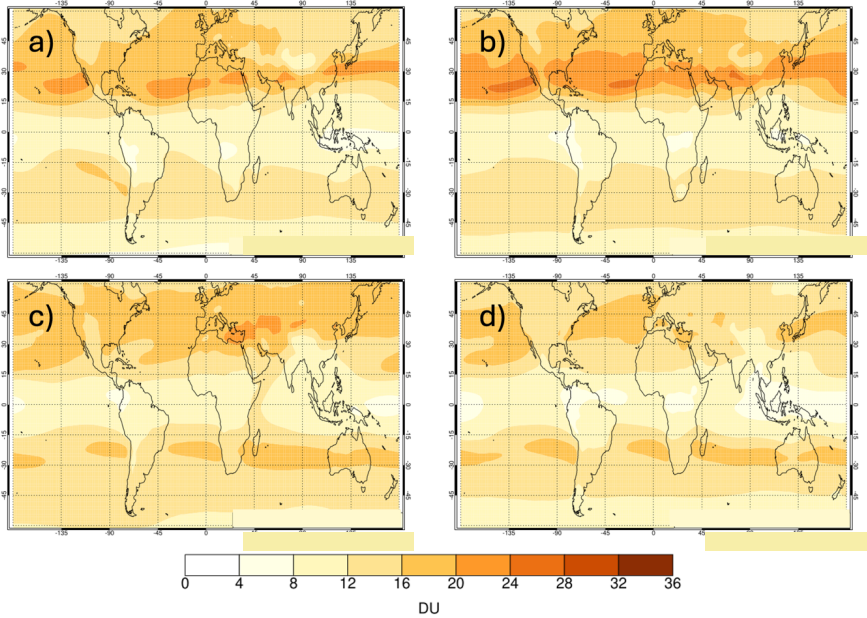
Deleted: 7

Deleted:

Deleted:

Deleted: 7

Deleted: b



Emissions regions for idealised tracers

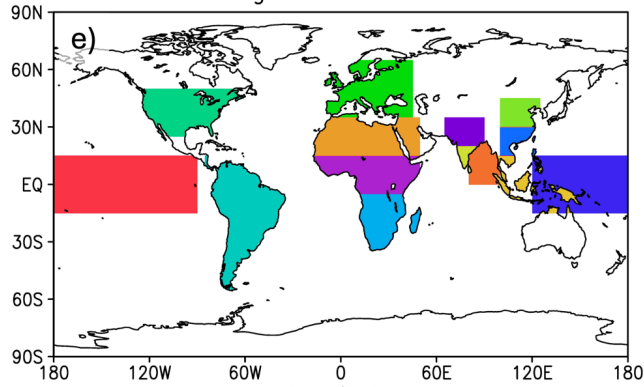
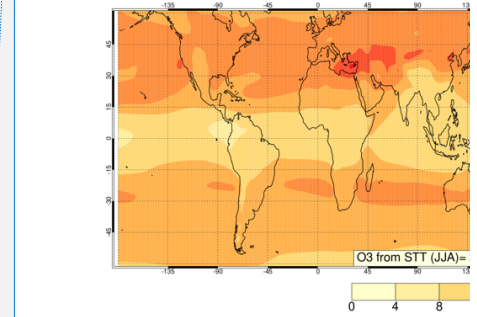
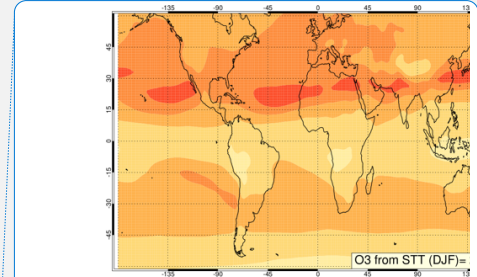
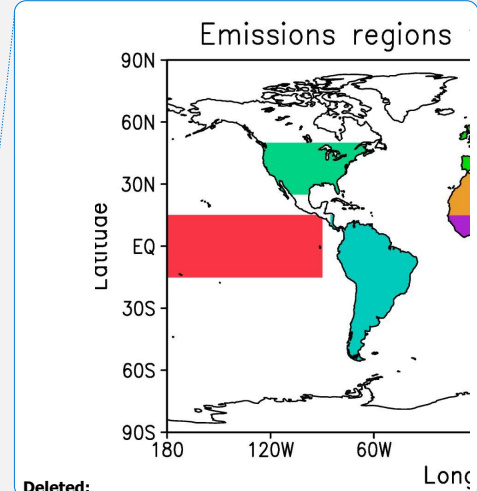


Figure 8. Integrated tropospheric column O_3_s tracer (in Dobson Units, DU) defined using prognostic ozone and the 2PV+380K tropopause, averaged over 2005-2017 using HIST1 and SCEN1 simulations (see Table 6 for details) for (a) December-January (DJF) (b) March-May



Deleted:



Deleted:

Deleted: 7

Deleted: a)

Deleted: for the

(MAM) (c) June-August (JJA) (d) September-November (SON), e) Emission regions for the 5 day and 30 day regional tracers.

Deleted: .
 Deleted: b
 Deleted: ¶ ... [6]

Table 6. Description of the UKESM1 model simulations.

Simulation	Nudging Dataset	Time Period	Notes	Rose suite ID
HIST1	ERA-Interim	1981-2014	Settings as per UKESM1.	u-bv711 (01/1981-11/1991) and u-bw316 (12/1991-12/2014)
HIST2	ERA-5	1982-2014	Includes code-changes described in Ranjithkumar et al. (2021)	u-bw784 (01/1982-12-2014)
HIST3	ERA-5	1982-2014	Includes code-changes described in Ranjithkumar et al. (2021), technical improvements to the top-boundary condition of the tracers, updated photolysis rates, and the improved heterogeneous chemistry of Dennison et al. (2019)	u-bv828 (01/1982-05/2008) and u-bx320 (06/2008-12/2014)
SCEN1	ERA-Interim	2015-2019	Continuation of HIST1	u-by117 (SSP3-7.0)
SCEN2	ERA-5	2015-2020	Continuation of HIST2	u-by803 (SSP3-7.0)
SCEN3	ERA-5	2015-2020	Continuation of HIST3	u-by808 (SSP3-7.0)

2.4.1 Data archive

892 Tb of UKESM1 model data were generated through the ACSIS project. A huge number of model diagnostics were output, including high time frequency fields (hourly) across the North Atlantic basin. These are listed here: <https://www.ukca.ac.uk/wiki/index.php/AC SIS/u-bv711/STASH>. Owing to the large nature of the model data set, selected core chemical species and tracers are available to download as monthly mean files from the CEDA dataset <https://data.ceda.ac.uk/badc/acsis/UKESM1-hindcasts>, Abraham (2024). These include ozone and ozone precursors (O₃, NO, NO₂, CO and methane) and the idealised tracers used to diagnose transport in the North Atlantic (four stratospheric tracers and thirty regionally emitted tracers). This data is available for all the model runs described in Table 6. The data is in Met Office PP format, which can be read using open access Python libraries held at <https://ncas-cms.github.io/cf-python>. If desired, users may also apply for a Met Office MASS (offline tape

Deleted: ,
 Deleted: t
 Deleted:

archive) account on the UK JASMIN data facility (<https://jasmin.ac.uk>) and search the Rose Suite IDs given in Table 6 for access to data from the specific experiments performed.

3 Ocean data sets

The North Atlantic Ocean is a major component of the overall North Atlantic Climate system and one of the key objectives of the ACSIS programme was to document the significant changes in ocean circulation and heat content which have taken place since the mid 20th century, to investigate the physical processes responsible and to identify their external drivers. Another objective was to understand how the ocean might change in the next several decades and to evaluate the potential impacts of these changes on human society and activities. In order to fulfil these objectives we compiled a substantial number of new data products and new model simulations.

The data products were compiled on the underlying principle of estimating components of the North Atlantic heat budget plus the sea surface temperature and sea surface height (dynamic and thermosteric) as these latter two are key to the wider impacts of the ocean on the atmosphere and on coastal sea level. Thus we brought together a new water mass preserving objectively interpolated ocean temperature and salinity dataset based on the international Argo float array described in Section 3.1 below (King, 2023) [with two basin scale observational estimates of the horizontal ocean volume and heat transports at 26°N and at ~55°N described in previous publications \(RAPID - <https://rapid.ac.uk/rapidmoc/>, McCarthy et al 2015; Moat et al., 2020\) and at ~55°N \(OSNAP - <https://www.ukosnap.org/>, Lozier et al., 2019\) and a new high spatial and temporal resolution Atlantic sea surface temperature dataset previously described by Williams and Berry \(2020\)](#). On the modelling side, we undertook new cutting edge NEMO forced ocean model simulations with a variety of surface forcing datasets at resolutions of 1/4° and 1/12°, described in Section 3.2 [complementary to similar coupled ocean-atmosphere integrations performed at both high and low atmospheric resolution \(previously published and described as an additional dataset in Section 5.2\)](#).

3.1 Ocean temperature and salinity, and upper ocean heat content

[In order to understand and quantify decadal climate variability and trends in the North Atlantic region, the NOC has produced new ocean temperature and salinity datasets based on the Argo float array using objectively mapped Argo profiles based on density levels, which preserve ocean water masses. \(Desbryères et al., 2017\)](#). The dataset covers the period 2004-present and extends to depths of up to 2000m. Two versions are available with spatial resolutions of 2° and 1° respectively. During ACSIS the main use of this dataset has been to calculate subtropical and subpolar heat content alongside other available estimates in order to understand the interannual to decadal variability of the North Atlantic heat budget.

Here we illustrate the subpolar Ocean heat content (SOHC), which is an indicator of long-term changes in the heat supply to the North Atlantic region (Fig. 9). Changes in SOHC are thought to be important precursors of Atlantic Multidecadal Variability (e.g. Sutton et al., 2018), and have been linked to changes in climate extremes, for example the number of Atlantic hurricanes (Dunstone et al., 2011). The ACSIS SOHC time series are integrated from the region between

Deleted: two basin scale observational estimates of the horizontal ocean volume and heat transports at 26°N described in previous publications (RAPID - <https://rapid.ac.uk/rapidmoc/>, McCarthy et al 2015; Moat et al., 2020) and at ~55°N (OSNAP - <https://www.ukosnap.org/>, Lozier et al., 2019), a new high spatial and temporal resolution Atlantic sea surface temperature dataset previously described by Williams and Berry (2020) and

Deleted:

Deleted: ¶

¶ Taken together, this new collection of model and observation based data has allowed us make significant advances in our understanding of North Atlantic variability including phenomena such as the impact of subpolar heat loss on the Atlantic Meridional Overturning Circulation (Megann et al., 2021a), the subpolar fingerprints of changes in the AMOC (Smeed et al., 2018), the origin of interannual changes in subpolar SST (Josey and Sinha 2022), the link between subpolar SST and European winter weather (Grist et al., 2019) and summer heat waves (Mecking et al., 2019), the relationship between decadal variability in surface and subsurface temperature (Moat et al., 2019) and the impact of subpolar freshwater input on the North Atlantic atmosphere (Oltmans et al., 2020) to name just a few of the studies enacted under ACSIS. ¶

Deleted: As part of ACSIS the NOC has produced new ocean temperature and salinity datasets based on the Argo float array using sophisticated optimal interpolation techniques which preserve ocean water masses.

Deleted: degrees

Deleted: degree

Deleted: ure

Deleted: 8

45°N to 67°N, and 80°W to 0E. The time series are calculated from gridded EN4.2.2 (Good et al., 2013) and Argo objectively mapped 1° x 1° temperature data sets (King, 2023). The SOHC calculated from the new dataset developed during ACSIS is shown in red (based only on Argo measurements) while another calculation using the standard Met Office product EN4 (based on Argo, hydrographic and remote sensing measurements) is shown in black. The two datasets agree well over the overlapping period 2004-present and the differences between the decadal filtered lines gives a useful indication of the uncertainty in the heat content estimates due to the method of calculation. [This dataset can be used in conjunction with RAPID and OSNAP and the new Williams and Berry \(2020\) SST dataset mentioned in the introduction to this section.](#)

Deleted: degree

Deleted:

3.1.1 Data archive

Objectively mapped temperature and salinity data and are available for download from BODC as self-describing NetCDF (<http://doi.org/10.5065/D6H70CW6>) files:

<https://doi.org/10.5285/fe8e524d-7f04-41f3-e053-6c86abc04d51> (King, 2023) as are upper ocean heat content timeseries, also in NetCDF format :<https://doi.org/10/g6wm>, <https://doi.org/10/g8g2> (Moat et al. (2021a-b)).

Deleted:

Deleted: et al.

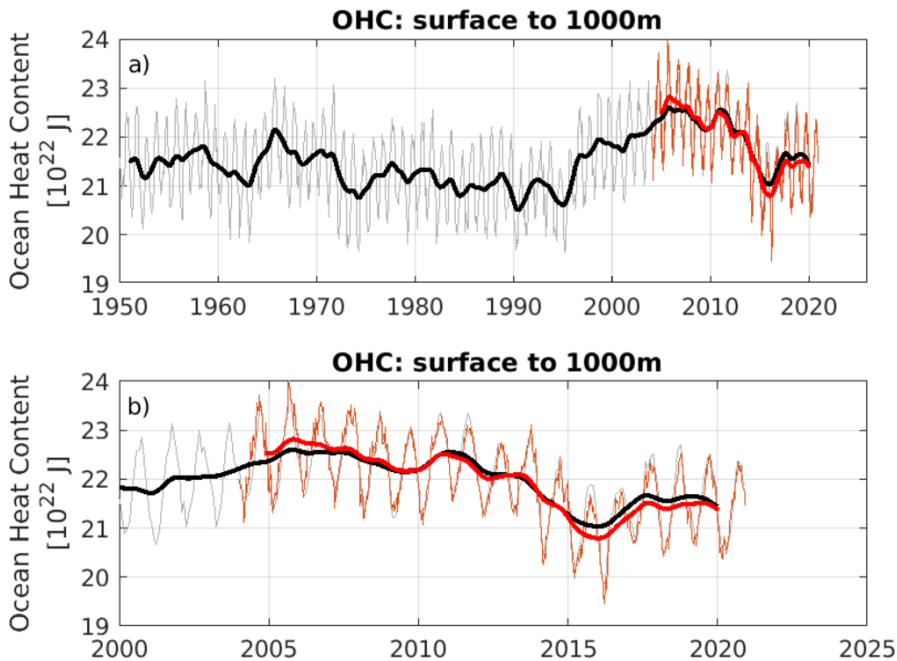


Figure 8. Subpolar ocean heat content index in units of 10^{22} J using EN4 (black) and ARGO OI (red) a) 1950-2020 and b) during the Argo period 2004-2020). Thick lines have a low pass filter applied with periods variability on periods shorter than 1.8 years removed.

3.2 Forced Ocean-ice simulations

Multiple forced ocean-ice simulations were run under ACSIS in order to elucidate the mechanisms of variability seen in the observations (e.g. Figure 9). A particular emphasis was placed on understanding how uncertainty in surface forcing (meteorological conditions such as windstress and air temperature) impacts predictions of climatically important processes such as the Atlantic Meridional Overturning Circulation (subsection 3.2.1). Another focus was on understanding the impact of modelling at higher (eddy resolving/eddy rich) horizontal resolution would have on the simulated ocean variability and trends compared to using standard (eddy permitting) resolution (subsection 3.2.2).

3.2.1 $1/4^\circ$ ocean models forced with three different surface meteorological datasets.

Three integrations of a global ocean and sea ice configuration, consisting of Global Ocean v6 (GO6, Storkey et al, 2018) and Global Sea Ice v8.1 (GSI8.1, Ridley et al, 2018) were carried out to provide a tool for scientific investigation of the mechanisms of variability of the AMOC and other modes of variability of the Atlantic Ocean. GO6 is based on NEMO v3.6 (Madec 2016), and GSI8.1 on CICE v5.2.1 (Hunke & Lipscomb, 2010; Ridley et al., 2018) The GO6 ocean configuration was chosen to be the same as that developed under the JMMP collaborative programme (<http://www.jwcrp.org.uk/under/jmmp.asp>) as the ocean component of the UK's submissions under CMIP6, namely GC3.1 (Williams et al., 2017) and UKESM1 (Sellar et al., 2019), and informed choices made in the UK OMIP (Ocean Model Intercomparison Project – Griffies et al., 2016) integrations. Three forcing datasets were used to assess the sensitivity of the models to the choice of forcing data. These were the CORE2 (Large and Yeager 2009), DFS5.2 (Brodeau et al 2010) and JRA-55 (Tsujino et al., 2018) datasets, each supplying gridded surface meteorological variables (air temperature, humidity, and surface winds at subdaily intervals), surface radiative fluxes (downwelling shortwave and longwave at daily intervals) and freshwater input (snow and precipitation at monthly intervals).

The simulations were run on a global domain on the eORCA025 $1/4^\circ$ grid, with 75 vertical levels. The integrations were run from 1958 to 2007 (CORE2); from 1958 to 2015 (DFS5.2) and from 1958 to 2020 (JRA-55), and monthly means are archived. Variables archived include full-depth potential temperature and salinity, horizontal and vertical velocity components, surface fluxes of heat, freshwater and momentum; mixed-layer depth, sea ice cover and thickness, but many other state and process variables were also archived. Note that sea ice files from the JRA-forced run are only available for years 1990-2001 and 2002-2020. These forced ocean-ice simulations use the same configuration as the ocean component of the coupled simulations described in section 5.2.

A comparison of the model drifts in globally averaged temperature and salinity is shown in fig. 10. The reason for showing model drifts is to alert users to the magnitude and sign of biases present in these model simulations. Biases exist in all model simulations and must be taken into account when using them to understand historical ocean circulation changes. There is a large

Deleted: Figure 8. Subpolar ocean heat content index in units of 10^{22} J using EN4 (black) and ARGO OI (red) a) 1950-2020 and b) during the Argo period 2004-2020). Thick lines have an annual low pass filter applied. ¶

Formatted: Font: Not Bold

Deleted: $1/4^\circ$

Deleted: , as a deliverable for Work Package 2.3 of ACSIS

Deleted: , intended

Deleted: heat

Deleted: . S

Deleted: 3

Deleted: 1

Deleted:

Deleted: ure

Deleted: 9

Deleted: In particular

Deleted: t

positive drift in upper ocean salinity in the DFS5.2 forced simulation (Fig 10(e)) and a relatively large freshening in the CORE2 simulation (Figure 10(d)). Overall the JRA55 forced simulation shows moderate drift in both variables (Figure 10(f)). This ensemble is thus suitable for understanding the impact of model biases on representation of historical ocean circulation variability. For example, simulated interannual to multidecadal changes to Atlantic Ocean circulation are similar between the models despite differences in the mean surface temperature and salinity (Fig 11). More details on the three simulations including their AMOC variability are given by Megann et al (2021a).

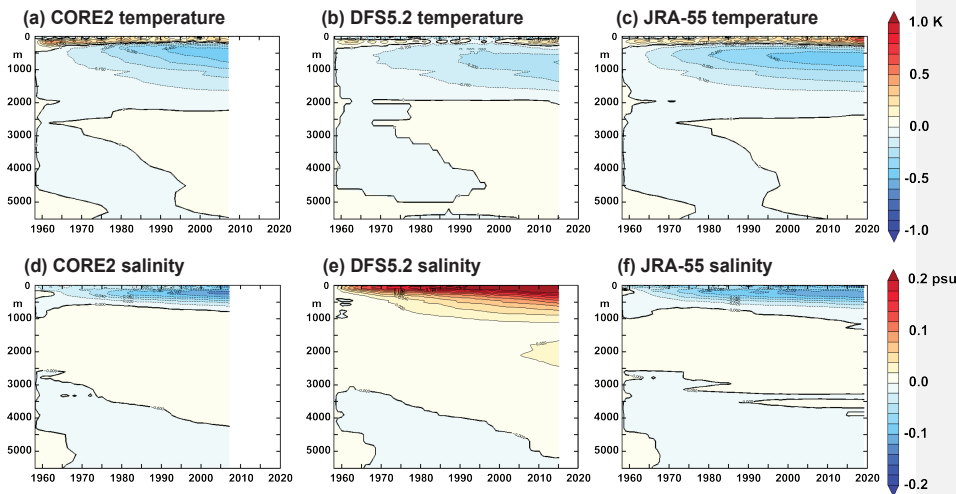


Figure 10. Annual drifts in global mean temperature (K), panels (a)-(c) and salinity (psu), panels (d)-(f), (bottom) as a function of depth in the ACSIS 1/4° forced ocean model simulations. (a), (d) are from the CORE2 forced simulation, (b), (e) are from the DFS5.2 forced simulation and (c), (f) are from the JRA-55 forced simulation.

Deleted: the
 Deleted: s
 Deleted: Nonetheless s
 Deleted: 0
 Deleted: and the
 Deleted: in the three simulations
 Deleted: We expect these simulations will be extremely useful to investigate the role of surface forcing in generating model biases and in determining the mean ocean circulation and its variability....

Deleted: 9
 Deleted: (top)
 Deleted:
 Deleted: Left panels
 Deleted: centre panels
 Deleted: right panels

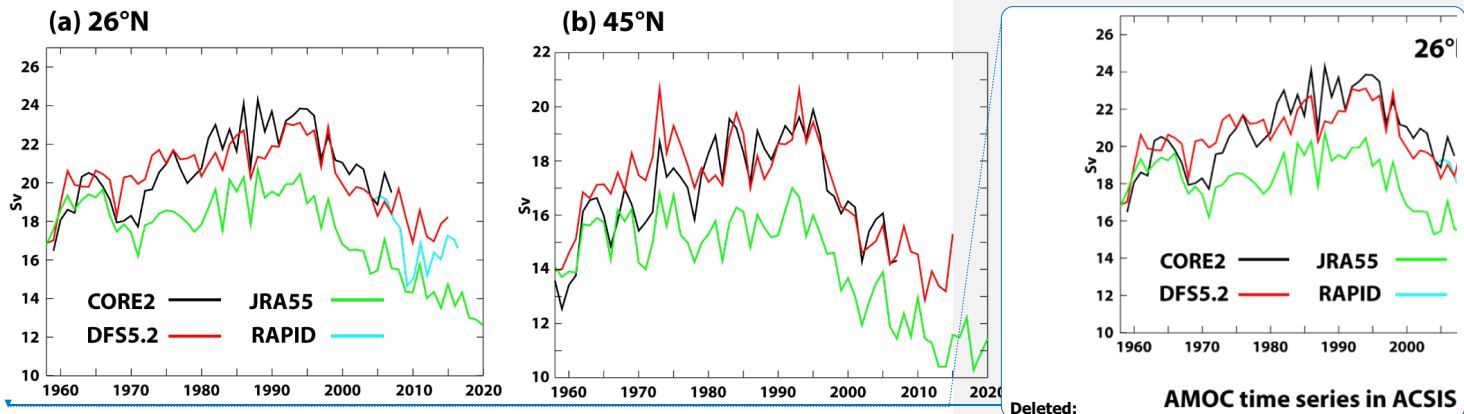


Figure 11. AMOC timeseries (Sv), 1960-2020 from the ACSIS $\frac{1}{4}^\circ$ forced ocean model simulations at (a) 26°N and (b) 45°N . Timeseries from all three integrations are shown on each panel: CORE2 forced simulation (black); DFS5.2 forced simulation (red) and JRA-55 forced simulation (green). The AMOC derived from observations at 26°N (the RAPID-MOCHA array), available from 2004 onwards, are plotted in cyan in panel (a).

3.2.2 $\frac{1}{4}^\circ$ and $1/12^\circ$ “twin” simulations

Two integrations of the Global Ocean v8p7 (GO8p7) ocean and sea ice configuration simulation were run under the ACSIS programme. This is based on NEMO v4.0.4 (Madec et al., 2019), including the SI3 sea ice model, and has been developed under the Joint Marine Modelling Programme (JMMP see <http://www.jwcrp.org.uk/under/jmmp.asp>). The simulations are identical apart from the ocean horizontal resolution: one on a $\frac{1}{4}^\circ$ grid, and the other a $1/12^\circ$ grid. They are forced with the JRA-55 surface forcing dataset (Tsujino et al., 2018) from 1958 to 2021. The integrations are intended to provide a tool for scientific investigation of the mechanisms of variability of the AMOC and ocean heat content of the Atlantic Ocean at an eddy-rich resolution. The GO8p7 configuration is close to that expected to be incorporated in the GC5.1 coupled climate model and the UKESM2 earth system model, both aimed at CMIP7. The configuration was implemented at the two resolutions, with the parameter and physics setting as close as possible (there are some necessary changes to lateral friction which are required for numerical stability at higher resolution), to investigate the sensitivity of the circulation, numerical mixing and other metrics to the resolution.

As for section 3.2.1 The integrations were carried out on a global domain on eORCA025 $1/4^\circ$ and eORCA12 $1/12^\circ$ grids, with 75 vertical levels. The integrations were run from 1958 to 2020 and monthly and annual means of the 3-D and 2-D model fields were saved (including full-depth potential temperature and salinity, horizontal and vertical velocity components, surface fluxes of heat, freshwater and momentum; mixed-layer depth, and sea ice cover and thickness). 5-day means of a selection of surface fields (including SST, mixed layer depth and sea-surface height) are also archived.

Deleted: Figure 10. AMOC timeseries (Sv), 1960-2020 from the ACSIS $\frac{1}{4}^\circ$ forced ocean model simulations at 26°N (left) and 45°N (right). Timeseries from all three integrations are shown on each panel: CORE2 forced simulation (black); DFS5.2 forced simulation (red) and JRA-55 forced simulation (green). The AMOC derived from observations at 26°N (the RAPID-MOCHA array), available from 2004 onwards, are plotted on the left panel (cyan).

Deleted:

Deleted: 4

Deleted: 4

Deleted: 12

To illustrate the simulations we show timeseries of some key globally integrated variables from the twin simulations and also, for context, from the three $\frac{1}{4}^\circ$ simulations already described in section 3.2.1 (Fig 12). Global mean temperature drifts are of order 0.05K over the ~50 year integrations or 0.001K yr^{-1} . The $\frac{1}{12}^\circ$ simulation has a smaller drift than its twin $\frac{1}{4}^\circ$ resolution. The twin simulations show positive temperature drift while the other simulations show a negative drift. We expect to see an SST warming trend under the influence of anthropogenic warming superimposed on interannual and decadal variability. All the simulations show strong interannual variability with about the same amplitude and timing, forced by interannual changes in wind stress and buoyancy forcing, and not influenced by global temperature and salinity drifts. On decadal and longer timescales the difference between variability, secular trends and model drifts can be blurred. The models all show a small reduction in global mean SST from initialisation to the late 1970s. The DFS5.2 forced simulation then continues to reduce its SST until the mid 1980s after which the SST remains more or less stable until about 2010, however all the other simulations increase their SST at a fairly steady rate throughout the 1980s, 90s and 2000s. From about 2010 onwards all the simulations experience strong surface warming. Globally integrated downward net surface heat flux (sum of turbulent and radiative components) is consistent with the global mean surface temperature evolution with a negative net surface flux in the early decades for the three simulations with different surface flux forcing and a positive net flux for the twin simulations. The net heat flux for the twin simulations is generally positive whereas for the other simulations it only becomes positive around the year 2000 and this is when the global mean temperature in those simulations starts to rise. The downward heat flux clearly shows the signals of large volcanic eruptions (Agung, 1964, el Chichon 1982 and Pinatubo 1991) as well as the 1997 El Nino event (see Balmaseda et al 2013). The sharp downward dip in 2009 is interesting and possibly linked to the sudden AMOC reduction at that time, but further research is required to investigate this. With the exception of the DFS5.2 forced simulations, global mean salinity and global mean surface salinity show quite small trends consistent with a reasonably balanced surface freshwater flux. The DFS5.2 forced simulation shows strong salinification consistent with a net loss of freshwater through the surface. The twin runs show best conservation of freshwater. Finally, the net heating/cooling and freshening/salinification of the simulations is reflected in the global mean sea surface height which is most stable in the twin simulations.

Deleted: 4

Deleted: 4

Deleted: 1

Deleted: degree

Deleted: f

Deleted: o

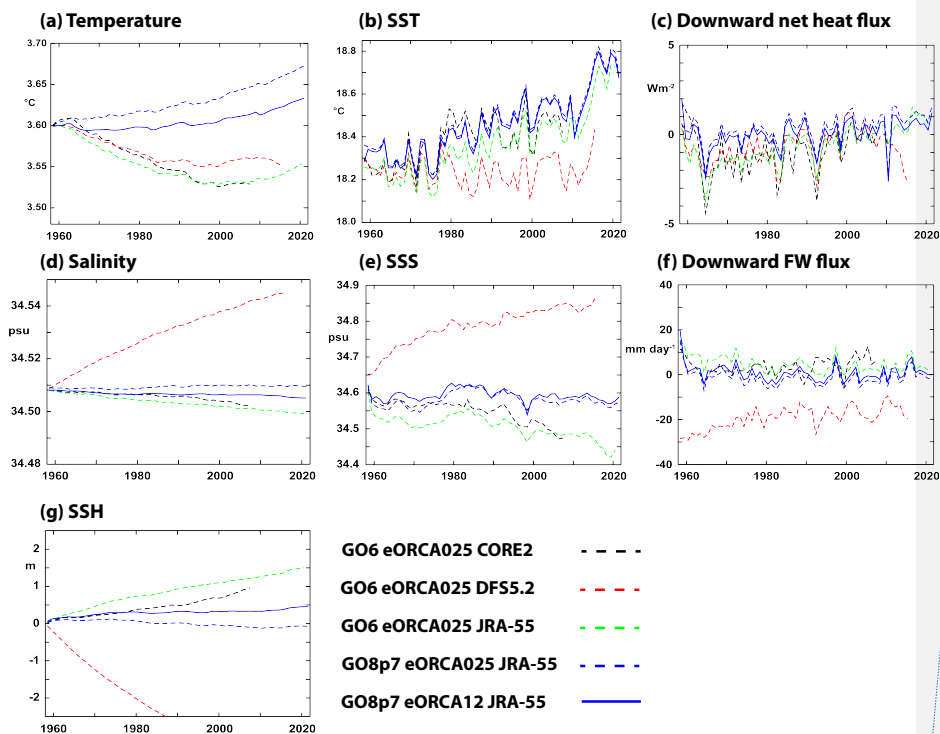
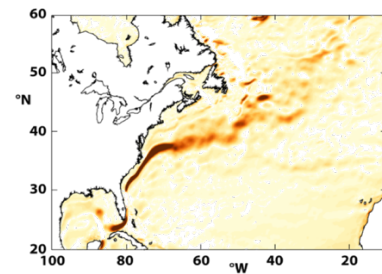
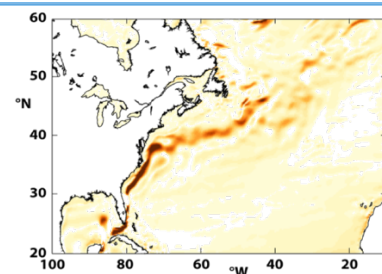


Figure 12. Time series of key variables in the ACSIS $1/4^\circ$ and $1/12^\circ$ forced ocean simulations. The variables plotted are: (a) global mean temperature; (b) global mean sea-surface temperature; (c) global mean net downward air-sea heat flux; (d) global mean salinity; (e) global mean sea-surface salinity; (f) downward freshwater flux; (g) global mean sea-surface height. Dashed lines are from the $1/4^\circ$ model (CORE2 forced – black, DFS5.2 forced – red, JRA-55 forced, $1/4^\circ$ twin simulation – blue) whilst the solid blue line is from the $1/12^\circ$ twin simulation. Note that the green and blue lines are all from JRA-55 forced model simulations but with different model code versions and configurations (see text).

Deleted: Figure 11. Time series of trends in key variables in the ACSIS $1/4^\circ$ and $1/12^\circ$ forced ocean simulations. The variables plotted are global mean temperature (top left), global mean sea-surface temperature (top centre), global mean net downward air-sea heat flux (top right), global mean salinity (second row left), global mean sea-surface salinity (second row centre), downward freshwater flux (second row right) and global mean sea-surface height (bottom left). Dashed lines are from the $1/4^\circ$ degree model (CORE2 forced – black, DFS5.2 forced – red, JRA-55 forced, $1/4^\circ$ twin simulation – blue) whilst the solid blue line is from the $1/12^\circ$ twin simulation. Note that the green and blue lines are both from JRA-55 forced model simulations but with different model code versions and configurations (see text).



Surface speed ($m s^{-1}$)

Surface circulation

Deleted:

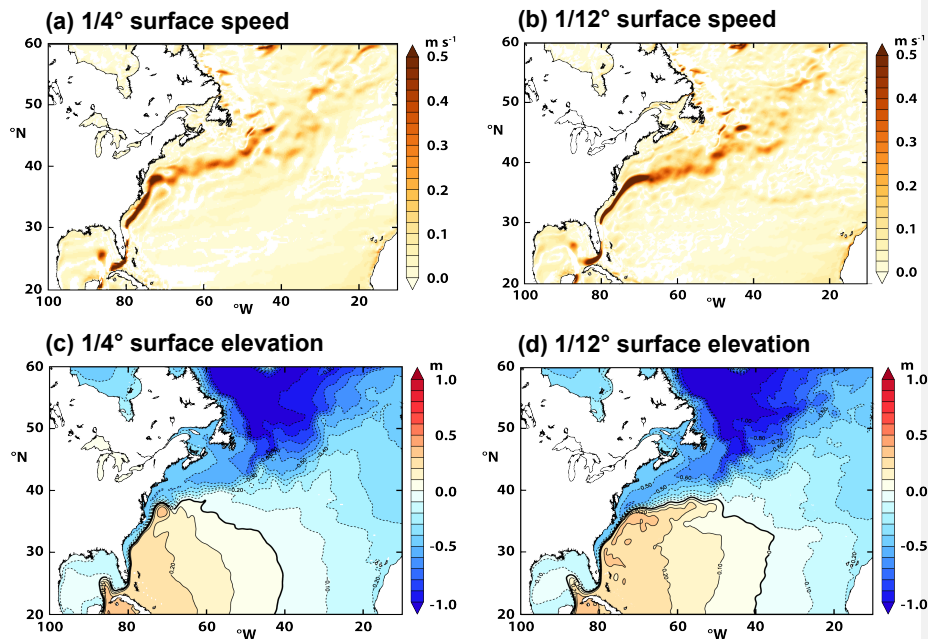


Figure 13. Surface North Atlantic circulation from the ACSIS GO8p7 twin simulations averaged over years 2000-2009. Surface speed in m s^{-1} for (a) the $1/4^\circ$ simulation and (b) for the $1/12^\circ$ simulation; and sea surface height in metres for (c) the $1/4^\circ$ simulation and (d) the $1/12^\circ$ simulation (bottom right). In panels (c) and (d) the global mean surface height has been subtracted to make comparison easier.

A final illustration shows the mean surface circulation in the North Atlantic from the twin simulations (Fig 13). The most obvious difference in the surface current speed (panels (a) and (b)) is that the Gulf Stream separation is more realistic in the $1/12^\circ$ simulation where the current moves northeastwards off Cape Hatteras ($\sim 38^\circ\text{N}$). This contrasts with the $1/4^\circ$ simulation where the current shifts direction anticlockwise to remain quite close to the coast. The kink in the Gulf Stream Extension at the Northwest corner ($\sim 50^\circ\text{W}$, 40°N) is also more realistic in the $1/12^\circ$ simulation and there is also a discernible signature of the Azores current (zonal feature around 34°N) which is extremely faint in the $1/4^\circ$ simulation. Similar features can be seen in the mean sea surface height from the two simulations (right panels). One interesting difference is in the penetration of the Labrador Current much further south in the $1/12^\circ$ simulation – where the low sea surface heights characteristic of the subpolar gyre penetrate south west along the North American shelf/slope region north of the Gulf stream extension (between 80°W and 50°W and 35°N to 45°N). Decadal variability in the position of the Gulf Stream has been shown to be linked to salinity anomalies that are advected southwards by the Labrador Current (New et al.,

Deleted: Figure 12. Surface North Atlantic circulation from the ACSIS twin simulations averaged over years 2000-2009. Anomalous surface current magnitude (m s^{-2}) for the $1/4^\circ$ simulation (top left) and for the $1/12^\circ$ simulation (bottom left), Anomalous mean sea surface height (m) for the $1/4^\circ$ simulation (top right) and the $1/12^\circ$ simulation (bottom right).¹

Deleted: 2

Deleted: velocity

Deleted: anomalies

Deleted: left hand

Deleted: $1/4^\circ$

Deleted: missing

Deleted: $1/4^\circ$

2022) so these differences between the simulations are likely to impact on their simulation of AMOC variability.

3.2.3 Data archive

Data from all the ocean simulations are archived in NetCDF format, with [four](#) separate files [for each month of simulation. Variables in NEMO are divided into four types which are discretised on slightly different numerical grids. known as the T-grid for tracers such as temperature and salinity, and the U, V and W grids for the corresponding components \(positive eastwards, northwards and upwards respectively\) of the 3D velocity \(Madec, 2016, 2019\).](#) Each variable has a long name which gives a detailed description of the variable (see Madec, 2016, 2019 for an explanation of the data output format). Separate monthly NetCDF files contain sea ice variables and [Lagrangian iceberg properties trajectories on the CICE grid.](#) The data are archived at CEDA (Megann et al., 2021b, c, d):

CORE2-forced run: <https://dx.doi.org/10.5285/119a5d4795c94d2e94f610647640edc0> (Megann et al., 2021b,

DFS5.2-forced run: <https://dx.doi.org/10.5285/a0708d25b4fc44c5ab1b06e12fef2f2e>, (Megann et al., 2021c)

JRA55-forced run: <https://dx.doi.org/10.5285/4c545155dfd145a1b02a5d0e577ae37d> (Megann et al., 2021d)

¼° “twin” simulation: <https://dx.doi.org/10.5285/e02c8424657846468c1ff3a5acd0b1ab> (Megann et al., 2022a)

1/12° “twin” simulation: <https://dx.doi.org/10.5285/399b0f762a004657a411a9ea7203493a> (Megann et al., 2022b).

4 Ice data sets.

4.1 Advanced Sea Ice model simulations

Results from 6 forced ocean-ice simulations and 2 stand-alone ice simulations are included to document the impact of sea ice physics and atmospheric forcing data on the Arctic sea ice evolution. All of them use the same sea ice model CICE configuration GSI8.1 (Ridley et al., 2018) and the ocean-ice simulations use the same ocean model NEMO GO6.0 (Storkey et al., 2018) as the forced ocean ice simulations of section [3.2](#), and the HadGEM3 climate model of section [5.2](#). Three different atmospheric forcing data set are applied: NCEP Reanalysis-2 (NCEP2) data (Kanamitsu et al., 2002, updated 2020), CORE2 surface data (Large & Yeager, 2009) and the atmospheric forcing data set DFS5.2 (Dussin et al., 2016). Regarding the sea ice component, we use the default CICE setup as in HadGEM3 (CICE-default) and an advanced setup (CICE-best) in which a new process is added (snow loss due to drifting snow) and some adjustments have been made to model physics and parameters. See Schroeder et al. (2019) and Table 7 for details.

Table 7. Overview of model simulations with default and improved sea ice processes.

Deleted: for

Deleted: v

Deleted: defined

Deleted: the T

Deleted: grids (one for each month of simulation) as is standard for NEMO

Deleted: l

Deleted: 4.4

Deleted: s

Deleted: 3

Deleted: 1

Simulation	Atmospheric forcing	Ocean model	CICE setup	Time period
CICE-default	NCEP2	Mixed-layer	CICEv5.1.2 with prognostic melt pond model and EAP rheology	1980-2020
CICE-best	NCEP2	Mixed-layer	As CICE-default, but with several modifications including snow drift scheme, bubbly conductivity scheme, increased sea ice emissivity and reduced melt pond max fraction parameter (see Schroeder et al., 2019)	1980-2020
NEMO-CICE-1deg-default-CORE	CORE II	NEMOv3.6	CICEv5.1.2 with prognostic melt pond model	1960-2009
NEMO-CICE-1deg-best-CORE	CORE II	NEMOv3.6	As CICE-best	1960-2009
NEMO-CICE-1deg-best-DFS	DFS5.2	NEMOv3.6	As CICE-best	1960-2015
NEMO-CICE-1deg-best-NCEP	NCEP2	NEMOv3.6	As CICE-best	2000-2020
NEMO-CICE-1/4deg-default-DFS	DFS5.2	NEMOv3.6	CICEv5.1.2 with prognostic melt pond model	1979-2015
NEMO-CICE-1/4deg-best-DFS	DFS5.2	NEMOv3.6	As CICE-best, but with increased ice and snow conductivity instead of snow drift scheme	1979-2015

The impact of our changes to the sea ice model on the fidelity of the model sea ice simulation is shown in Figure 14. All simulations with the default CICE setup (thin lines) underestimate the mean Arctic sea ice thickness during winter. Figure 14 shows that the mean Arctic CryoSat-2 sea ice thickness is more than 50cm thicker in April than in those simulations (see Section 5.3 for the source of our ice thickness estimates). By applying the advanced CICE setup, all simulations (stand-alone, NEMO-CICE 1° and NEMO-CICE 1/4°, thick lines) show realistic mean April sea ice thickness. The advanced setup leads to improvements in simulating summer sea ice extent, too (not shown) and highlights the importance of sea ice physics for accurate model simulations for the Arctic.

Deleted: 3

Deleted: 3

Deleted: y

Deleted: s

4.2 Data archive

Deleted: 1.1

Data from the global ocean simulations with advanced sea ice are archived in NetCDF format as described in section 3.2.3 above. Standalone sea ice simulations are similar, but output consist of a single NetCDF file containing sea ice variables on the CICE grid for each month of simulation. The data is accessible via CEDA: <http://catalogue.ceda.ac.uk/uuid/770a885a8bc34d51ad71e87ef346d6a8> (see Megann et al., 2021e).

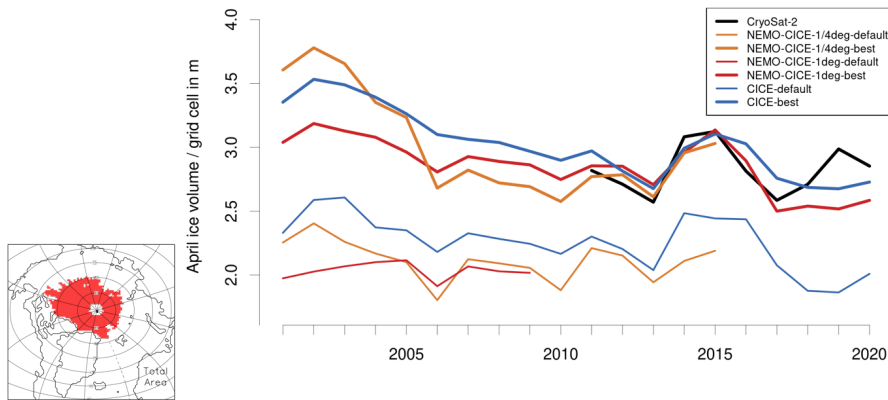


Figure 14. Mean April Arctic Sea ice volume per grid cell area over red region for several model simulations in comparison to CryoSat-2 estimates. CryoSat-2 thickness are multiplied with sea ice concentration from SSM/I with NASA-Team Bootstrap algorithm (Comiso, 2017). The selected region represents the area over which CryoSat-2 data are available for the whole period from 2010 to 2020 (October to April). Table 7 provides more information about the setup of the model simulations.

5. Synergies with Previously Published Work

The new datasets described in the previous sections should be viewed in the context of (and potentially used in conjunction with) several other datasets generated in whole or in part by the ACSIS programme and already published and described in the scientific literature. Here we provide a [very](#) brief overview of these other datasets and include links to where they can be accessed. [The subsections below correspond to the preceding sections on atmospheric composition \(subsection 5.1 corresponding to Section 2\) Ocean observations and model simulations \(subsections 5.2 corresponding to Section 3\) and sea ice model simulations \(subsection 5.3 corresponding to Section 4\).](#)

5.1 Stratospheric Aerosol Surface Area Density from Explosive Volcanic Eruptions

The “MajorVolc” datasets are model simulations [within the high-top N96L85 GA4 UM-UKCA composition-climate model \(Walters et al., 2014\)](#) of the monthly progression of the volcanic aerosol clouds from the 3 largest volcanic eruptions of the 20th century – 1963 Agung, 1982 El Chichon and 1991 Pinatubo. [The latter two eruptions fell within the period covered by the UKESM simulations described in Section 2.4, so could be useful in interpreting the aerosol distributions in those simulations.](#) The simulations are based on the [Historical Eruption SO₂ Emission Assessment \(HErSEA\) experiment protocol \(Timmreck et al., 2018\)](#). They apply the v8.2 of the GLOMAP-mode aerosol microphysics module (Mann et al., 2010; Dhomse et al., 2014; Mann et al., 2015; Brooke et al., 2017; Dhomse et al., 2020) [and improve on the CMIP6 volcanic aerosol dataset \(Arfeuille et al., 2013; Luo, 2016\)](#). The datasets are described by

Formatted: Font: (Default) +Headings (Calibri)

Formatted: Font: (Default) +Headings (Calibri), 10 pt

Formatted: Font: (Default) +Headings (Calibri)

Formatted: Font: (Default) +Headings (Calibri), 10 pt

Formatted: Font: (Default) +Headings (Calibri)

Deleted: Figure 13. Mean April Arctic Sea ice volume over red region for several model simulations in comparison to CryoSat-2 estimates. The selected region represents the area over which CryoSat-2 data are available for the whole period from 2010 to 2020 (October to April). Table 7 provides more information about the setup of the model simulations.

Deleted: Previously published ACSIS datasets

Deleted: UM-UKCA volcanic aerosol

Deleted:

Deleted: The interactive stratospheric aerosol model experiments break new ground, being an advance on the 2D global aerosol model simulations that generated the CMIP6 volcanic aerosol dataset (Arfeuille et al., 2013; Luo, 2016), the stratospheric circulation and dynamics progressing in 3D, within the high-top N96L85 GA4 UM-UKCA composition-climate model (Walters et al., 2014).

Deleted:) including recent adaptations for the stratosphere (

Deleted: . This upgraded capability predicts the volcanic forcings with very high fidelity, each of the steps in the formation, growth and sedimentation of the sulphuric acid aerosol particles, the UM-UKCA model also calculating the oxidation rate of the volcanic SO₂, consistently with the depletion and replenishment of oxidants that occurs for the amount of SO₂ emitted.

Dhomse (2020). Dataset identifiers are: <https://doi.org/10.17632/n3g2htz9hk.1> (Dhomse (2020)), <https://doi.org/10.5281/zenodo.4739170> for Pinatubo (Feng et al., 2021); <https://doi.org/10.5281/zenodo.4744633> for El Chichon (Dhomse et al., 2021a)); <https://doi.org/10.5281/zenodo.4744686> for Agung (Dhomse et al., 2021b)).

5.2 CMIP6 HighResMIP global climate model simulations

All the model and observations based datasets described in Sections 2-4 may be placed in the context of the 6th Coupled Model Intercomparison Project (CMIP6) HighResMIP (<https://www.highresmip.org/>) sub project (Haarsma et al. 2016, Roberts et al. 2018). The UK contribution to this subproject was based on the HadGEM3 global climate model (Hewitt et al 2011), with a resolution of ~50 km in the atmosphere and ~0.25° in the ocean, and was delivered as part of the EU Horizon 2020 PRIMAVERA project (<https://www.primavera-h2020.eu/>). The NEMO ocean component in these simulations is the same configuration as the forced ocean model simulations described in section 3.2. The HadGEM3 PRIMAVERA simulations most relevant to this paper were atmosphere only simulations with horizontal resolutions of N256 (~50km) (Roberts (2017a), <http://doi.org/10.22033/ESGF/CMIP6.6029> and Roberts (2019a), <http://doi.org/10.22033/ESGF/CMIP6.6013>) and N512 (~25km) (Roberts (2017b), <http://doi.org/10.22033/ESGF/CMIP6.6024> and Roberts (2019b), <http://doi.org/10.22033/ESGF/CMIP6.6008>) and analogous fully coupled simulations with an ocean resolution of 1/4° (Roberts (2018a), <http://doi.org/10.22033/ESGF/CMIP6.6040>, Roberts (2019c), <http://doi.org/10.22033/ESGF/CMIP6.5984c>, and Schiemann et al. (2019a), b, <http://doi.org/10.22033/ESGF/CMIP6.6041>, <http://doi.org/10.22033/ESGF/CMIP6.5985>). The simulations were conducted in pairs consisting of a historical simulation from 1950-2014 and a future simulation from 2015-2050. Two further cutting edge simulations were performed at even higher resolution in both ocean and atmosphere, 1/12°, and ~25km (N512) respectively (Roberts (2018b), <https://doi.org/10.22033/ESGF/CMIP6.5881>, and Roberts and Coward (2018) <https://doi.org/10.22033/ESGF/CMIP6.1822>). The first was a control 1950s climate running from 1950-2014 and the second was a future simulation (SSP5-8.5) from 2015-2050. Roberts et al., (2020) provide an assessment of the simulated Atlantic Meridional Overturning Circulation in this and other HighResMIP simulations.

5.3 Ice observations

Pan-Arctic sea ice thickness is estimated using satellite data from ESA's CryoSat-2 (CS2) mission. Launched in 2010, CryoSat-2's main payload is a Ku-band radar altimeter (SIRAL), which measures the elevation of Earth's surface. Sea ice freeboard (the portion of an ice floe above the waterline) is measured by differencing the elevation of the sea ice floe and that of the surrounding ocean. Sea ice freeboard is then converted to thickness by assuming that sea ice floats in hydrostatic equilibrium in the ocean, and assuming values for snow depth, and snow, ice and ocean density. CryoSat-2's orbit repeats every ~30 days, providing Arctic-wide sea ice thickness estimates every month from October-April. The method and dataset are detailed in full in Tilling et al., (2018), and monthly sea ice thickness, gridded at 5km, are available from the CPOM data portal <http://www.cpom.ucl.ac.uk/csopr/seaice.php>.

Deleted: ¶

Within ACSIS, the volcanic forcings were published as monthly-varying global 2D zonal-mean datasets for 4 key aerosol properties (stratospheric AOD, surface area density, particle effective radius, aerosol extinction at 550nm & 1020nm) on an open-access data archive (Dhomse, 2020). The variables align directly with Figures in the peer-reviewed journal article (Dhomse et al., 2020), and retain the 2 key... [7]

Deleted: .

Deleted: ¶

Deleted:)

Deleted: El Chichon (

Deleted: Agung (

Deleted: T

Deleted:

Deleted: aimed to increase the

Deleted: atmosphere and ocean

Deleted: global climate models to at least

Deleted: , and to assess the effect of these increases in... [9]

Deleted: The UK contribution to CMIP6 HighResMIP, (... [10]

Deleted: Some of the HadGEM3 PRIMAVERA simulat... [11]

Formatted: Default Paragraph Font

Formatted: Default Paragraph Font

Formatted: Default Paragraph Font

Deleted: (Table 8, rows 1-12),

Formatted: Default Paragraph Font

Deleted: 0.25 degrees

Deleted: Table 8, rows 13-24

Formatted: Default Paragraph Font

Formatted: Default Paragraph Font

Formatted: Default Paragraph Font

Formatted: Default Paragraph Font

Formatted: Default Paragraph Font

Formatted: Default Paragraph Font

Deleted:).

Deleted: The terminology is detailed in Haarsma et al. (... [12]

Deleted: 50

Deleted: Table 8, rows 25-26

Formatted: Default Paragraph Font

Formatted: Default Paragraph Font

Formatted: Default Paragraph Font

Deleted:)

Deleted: See

Deleted: for

Deleted: Table 8. Summary of HighResMIP global clim... [13]

For the purposes of the ACSIS project, we binned individual CryoSat-2 sea ice thickness estimates provided by CPOM into the five default ice thickness categories of the sea ice model CICE on a rectangular 50 km grid: (1) ice thickness $h < 0.6$ m, (2) $0.6 \text{ m} < h < 1.4$ m, (3) $1.4 \text{ m} < h < 2.4$ m, (4) $2.4 \text{ m} < h < 3.6$ m, and (5) $h > 3.6$ m (Schroeder et al, 2019). The mean area fraction and mean thickness are then derived for each thickness category. One of the key motivations of binning the CS2 along-track data into sub-grid ice thickness classes is to assess the role of the ice thickness distribution (ITD) in model initialisation and to quantify the realism of the CS2 ITD against independent estimates from airborne data. In addition to the bespoke data described above, monthly (October-April, 2010-2021) 5km-gridded sea ice thickness estimates are available (in ASCII and NetCDF formats) on the CPOM data portal: <http://www.cpom.ucl.ac.uk/csopr/seaice.php>.

6 Summary

We have described the multidisciplinary model and observational datasets that were produced by the UK ACSIS programme and how and where the data can be accessed. The scope of ACSIS was very broad, covering atmospheric composition, atmospheric circulation, ocean circulation, ice sheets ([not covered in this paper](#)), sea ice, and their interactions, and this breadth is reflected in the rich variety of datasets generated. We note that whilst the focus of the ACSIS programme was the North Atlantic, most of the model products covered the global domain, and many of the observational products have both global and regional significance. Despite its great size and scope, the ACSIS programme had finite resources and so was not able to fully exploit the data it generated. The landmark ACSIS papers cited here can be seen as starting points for further research. Therefore, we believe there is a major opportunity to repurpose our data for new research studies to build on the substantial financial and intellectual investment that ACSIS represents, and we express the hope that the ACSIS datasets provide a lasting legacy to the international environmental science community.

Appendix A: Overview of select aircraft composition instruments

UoM Time of Flight Chemical Ionisation Mass Spectrometer

The University of Manchester High Resolution-Time of Flight-Chemical Ionisation Mass Spectrometer (ToF-CIMS) is described in detail by Matthews et al., (2013) for aircraft deployment. Briefly, iodide ions cluster with sample gases in the ion-molecule reaction region (IMR) region creating a stable adduct. The flow is then sampled through a critical orifice into the first of the four differentially pumped chambers in the TOF-CIMS, the short segmented quadrupole (SSQ). Quadrupole ion guides transmit the ions through these stages. The ions are then subsequently pulsed into the drift region of the ToF-CIMS where the arrival time is detected with a pair of microchannel plate detectors with an average mass resolution of 4000 ($m/\Delta m$). The inlet design is an atmospheric pressure, rearward facing, short residence time inlet, consisting of 3/8" diameter polytetrafluoroethylene (PTFE) tubing with a total length to the instrument of 48 cm. A constant flow of 12 SLM is mass flow controlled to the ion-molecule reaction region (IMR) using a rotary vane pump (Picolino VTE-3). 1 SLM is then subsampled into the IMR for measurement.

Deleted: ,

Deleted: been

An Iris system as described by Lee et al. (2018) was employed to pressurise and mass flow control the sample flow into the instrument, avoiding sensitivity changes that would be associated with variations in pressure inflight that is not controlled sufficiently by the constant flow inlet. This works upon the principle of the manipulation of the size of the critical orifice in response to changes in the IMR pressure. As with the Lee et al., (2018) design, this works by having a stainless steel plate with a critical orifice and a movable PTFE plate on top of this, also with a critical orifice. These orifices either align fully and allow maximum flow into the instrument or misalign to reduce flow. This movement is controlled by the 24VDC output of the IMR Pirani pressure gauge in relation to the set point and was designed collaboratively with Aerodyne Research Inc. The IMR set point was 72 ± 3 mbar for the aircraft campaigns which is set through a combination of pumping capacity on the region (Agilent IDP3), mass flow controlled reagent ion flow and sample flow. The reagent ion flow is 1 SLM of ultra-high purity (UHP) nitrogen mixed with 2 SCCM of a pressurised known concentration gas mix of CH₃I in nitrogen, passed through the radioactive source, ²¹⁰Po. The total flow through the IMR is measured (MKS MFM) at the exhaust of the Agilent IDP3 pump so that not only is the IMR pressure monitored but also the sample flow. All mass flow controllers and mass flow meters are measured and controlled using the standard Aerodyne Inc EyeOn control unit and software.

A pressure controller is also employed on the short segmented quadrupole (SSQ) region to make subtle adjustments in this region independently of any small IMR changes that may occur inflight. This works upon the principle controlling an electrically actuated solenoid valve in a feedback loop with the SSQ pressure gauge to actively control a leak of air into the SSQ pumping line. The SSQ is pumped using an Ebara PDV 250 pump and held at 1.8 ± 0.01 mbar.

Instrument backgrounds are programmatically run for 6 seconds every minute for the entire flight, by overflowing the inlet with ultra high purity (UHP) nitrogen at the point of entry into the IMR. Here a 1/16th inch PTFE line enters through the movable PTFE top plate, ensuring that the flow exceeds that of the sample flow. Inlet backgrounds are also run multiple times during campaigns manually by overflowing as close to the end of the inlet as possible with UHP nitrogen. Data is taken at 4Hz during a flight, which is routinely averaged to 1 Hz for analysis. Of the 6 points in each background, the first 2 and last point are unused and the mean of the background is calculated using custom python scripting. Backgrounds are humidity corrected and using linear interpolation, a time series of the instrument background is determined and then subtracted to give the final time series (Matthews, 2023).

UoM Aerosol Mass Spectrometer

The chemical composition of non-refractory submicron aerosols (organic (OA), sulphate, nitrate, ammonium and non-sea-salt chloride) can be measured by a compact time-of-flight Aerosol Mass Spectrometer (C-ToF-AMS, Aerodyne Research Inc, Billerica, MA, USA) (Drewnick et al., 2005), which provides chemical characterization across a range of ion mass-to-charge (m/z) ratios from 10 to 500. The detailed operation of the AMS, including calibration and correction factors, during aircraft deployment has been described previously (Morgan et al., 2009). In brief,

aerosols enter the instrument via an aerodynamic lens inlet, focusing the incoming particles into a narrow beam. The aerodynamic lens system of the AMS in this study is tailored to sample submicron aerosols. Particles exit the aerodynamic lens into the particle-sizing chamber, which is evacuated to progressively lower pressures as the particle beam passes through and removes the majority of the gaseous material. Non-refractory components of the particles are then flash vaporised on a resistively heated porous tungsten surface. The resultant gaseous molecules are ionised by a 70-eV electron beam released from a tungsten filament. These fragment ions are analysed by a Time-of-Flight mass spectrometer (ToF-MS). The AMS mass spectra were recorded every 8 or 15 s during the ACSIS campaign (ACIS-1 and 3-6). The AMS data was processed using the standard SQUIRREL (SeQUential Igor data RetRIeval, v.1.65C) ToF-AMS software package. The AMS data was also calibrated using monodisperse ammonium nitrate and ammonium sulfate particles. A time- and composition-dependent collection efficiency (CE) was applied to the data based on the algorithm by Middlebrook et al. (2012).

UoY LIF-SO₂

The University of York LIF-SO₂ instrument is a custom-built system for the highly sensitive detection of SO₂ via laser-induced fluorescence, and is based on the system originally demonstrated by Rollins et al. (2016). The basic operating principle is the excitation of SO₂ at 216.9 nm, generated from the fifth harmonic of a custom-built tuneable fibre-amplified semiconductor diode laser system at 1084.5 nm, and the subsequent detection of the resultant fluorescence photons. The laser wavelength is rapidly (~10 Hz) tuned on and off a strong SO₂ transition, with the difference between these signals being directly proportional to the SO₂ concentration within the sample cell. The laser wavelength is tracked using a reference cell containing a known SO₂ concentration.

The ACSIS-7 experiment was part of the first field deployment for the York LIF-SO₂, and was thus in part a learning experience on the operation of the instrument aboard an aircraft. The sample flow rate was maintained at 2 slpm and the use of a ram inlet allowed both the sample and reference cells to be operated at 400 mbar for the full altitude range of the campaign to maximise instrument sensitivity. Multi-point calibrations were carried out across the expected concentration range approximately every half an hour to ensure the instrument sensitivity was well characterised. To assess the possible quenching effect of excited SO₂ by water vapour, or increased wall losses when sampling humid air, calibrations in both stable ambient air and dry zero air were carried out, for which this effect proved negligible. The uncertainty in the LIF-SO₂ measurements was calculated predominantly from the uncertainty in the instrument sensitivity (typically 6 %). However, due to inconsistencies in the laser power and laser linewidth, the sensitivity was seen to vary during the course of each flight. Therefore, a mean sensitivity has

been applied and this variation has been conservatively added to the sensitivity uncertainty on a flight-by-flight basis to give an overall uncertainty of ~ 15 % (using the mean of this variation). The 3σ precision of 225 ppt has also been determined conservatively from stable ambient measurements due to issues with completely overflowing the instrument inlet with zero air in flight.

Code/Data availability

Code availability is not applicable for this article. All data is deposited in reliable data repositories and access is detailed in Table 1 of this article. [However, the programs and scripts used for plotting the Figures in this article are stored in a Zenodo repository: 10.5281/zenodo.13972336.](#)

Author contributions

ATA and BS prepared the original draft with input from TJB, LJC, EM, KR, MRR, FAS, KR, LT, LW, HW, MY

BS, EM and MRR edited the original draft, all authors reviewed the manuscript.

SJJB, TJB, EM, CR, FAS, LT, NT, LW, HW acquired data.

ATA, LJC, HC, PE, JL, BS, MY, acquired funding

Competing interests

There are no competing interests.

Acknowledgements

We gratefully acknowledge the financial support provided by the UK Natural Environment Research Council for the extensive data provided by the ACSIS project. Airborne data were obtained using the BAe-146 Atmospheric Research Aircraft flown by Airtask Ltd and managed by FAAM Airborne Laboratory, jointly operated by UK Research and Innovation and the University of Leeds. We would like to give special thanks to the Airtask pilots and engineers and all staff at FAAM Airborne Laboratory for their hard work in helping plan and execute successful flight campaigns during ACSIS. PE and LT were supported by NERC awards NE/T008555/1 and NE/S007458/1 for the development and operation of the LIF-SO₂. MY, TB, and the Penlee Point Atmospheric Observatory measurements were supported by the NERC projects ACSIS (NE/N018044/1) and MOYA (NE/N015932/1). TS and the Plymouth sunphotometer measurements were supported by the NERC project ACRUISE (NE/S005390/1) and by the Western Channel Observatory, which is funded by NERC through its National Capability Long-term Single Centre Science Programme, Climate Linked Atlantic Sector Science (NE/R015953/1). We further thank Frances Hopkins, Jani Pewter, Daniel Phillips, and Simone

Louw for instrument maintenance at Penlee Point Atmospheric Observatory. We thank Luis Neves, Instituto Nacional de Meteorologia e Geofísica, São Vicente (INMG), Mindelo, Cabo Verde and, Shalini Punjabi, WACL, for technical assistance in the CVAO measurements. Model simulations were performed at NCAS, NOC and CPOM under ACSIS grants NE/N018001/1 and NE/N018044/1.

References

Abalos, M., Orbe, C., Kinnison, D. E., Plummer, D., Oman, L. D., Jöckel, P., Morgenstern, O., Garcia, R. R., Zeng, G., Stone, K. A., and Dameris, M.: Future trends in stratosphere-to-troposphere transport in CCM1 models, *Atmos. Chem. Phys.*, 20, 6883–6901, <https://doi.org/10.5194/acp-20-6883-2020>, 2020.

Abraham, L.: Data provided by UKESM1 Hindcast simulations for the North Atlantic Climate System Integrated Study (ACSIS). accessed 31 January 2024, <https://data.ceda.ac.uk/badc/accis/UKESM1-hindcasts>, 2024.

Andersen, S. T. and Nelson, B. S. and Read, K. A. and Punjabi, S. and Neves, L. and Rowlinson, M. J. and Hopkins, J. and Sherwen, T. and Whalley, L. K. and Lee, J. D. and Carpenter, L. J.: Fundamental oxidation processes in the remote marine atmosphere investigated using the NO-NO₂-O₃ photostationary state, *Atmospheric Chemistry and Physics*, 22, (24) 15747–15765, <https://doi.org/10.5194/acp-22-15747-2022>, 2022.

Archibald, A.T., Folberth, G., Wade, D.C. and Scott, D.: A world avoided: impacts of changes in anthropogenic emissions on the burden and effects of air pollutants in Europe and North America, *Faraday Discussions*, 200, pp.475-500, 2017.

Archibald, A.T., M O'Connor, F., Luke Abraham, N., Archer-Nicholls, S., P Chipperfield, M., Dalvi, M., A Folberth, G., Dennison, F., S Dhomse, S., T Griffiths, P., Hardacre, C., J Hewitt, A., S Hill, R., E Johnson, C., Keeble, J., O Köhler, M., Morgenstern, O., P Mulcahy, J., Ordóñez, C., J Pope, R., T Rumbold, S., R Russo, M., H Savage, N., Sellar, A., Stringer, M., T Turnock, S., Wild, O. and Zeng, G.: Description and evaluation of the UKCA stratosphere-troposphere chemistry scheme (StratTrop v1.0) implemented in UKESM1, *Geosci. Model Dev.*, <https://doi.org/10.5194/gmd-13-1223-2020>, 2020.

Arfeuille, F. et al.: Volcanic forcing for climate modeling: a new microphysics-based data set covering years 1600–present, *Climate of the Past*, 10, 359–375, <https://doi.org/10.5194/cp-10-359-2014>, 2014.

Balmaseda M. A., Trenberth K. E., Källén E.: Distinctive climate signals in reanalysis of global ocean heat content, *Geophysical Res. Lett.* 40 (9), 1754–1759, <https://doi.org/10.1002/grl.50382>, 2013.

Behrenfeld, M. J., Moore, R. H., Hostetler, C. A., Graff, J., Gaube, P., Russell, L. M., Chen, G., Doney, S. C., Giovannoni, S., Liu, H., Proctor, C., Bolaños, L. M., Baetge, N., Davie-Martin, C., Westberry, T. K., Bates, T. S., Bell, T. G., Bidle, K. D., Boss, E. S., Brooks, S. D., Cairns, B., Carlson, C., Halsey, K., Harvey, E. L., Hu, C., Karp-Boss, L., Kleb, M., Menden-Deuer, S., Morison, F., Quinn, P. K., Scarino, A. J., Anderson, B., Chowdhary, J., Crosbie, E., Ferrare, R., Hair, J. W., Hu, Y., Janz, S., Redemann, J., Saltzman, E., Shook, M., Siegel, D. A., Wisthaler, A., Martin, M. Y., and Ziemba, L.: The North Atlantic Aerosol and Marine Ecosystem

Deleted: Andersen, S. T., Carpenter, L. J., Nelson, B. S., Neves, L., Read, K. A., Reed, C., Ward, M., Rowlinson, M. J., and Lee, J. D.: Long-term NO_x measurements in the remote marine tropical troposphere, *Atmos. Meas. Tech.*, 14, 3071–3085, <https://doi.org/10.5194/amt-14-3071-2021>, 2021.

Deleted: ¶

... [14]

Study (NAAMES): Science Motive and Mission Overview, *Front, Mar. Sci.*, 6, 122, <https://doi.org/10.3389/fmars.2019.00122>, 2019.

Boylan, P., Helmig, D., Oltmans, S. and Miller, L.A.: Ozone in the Atlantic Ocean marine boundary layer, *Elementa: Science of the Anthropocene*, 3, 000045, <https://doi.org/10.12952/journal.elementa.000045>, 2015.

Brodeau, L. Barnier, B., Treguier, A.-M., Penduff, T., Gulev, S.: An ERA40-based atmospheric forcing for global ocean circulation models. *Ocean Modelling* 31 (2010) 88–104 ISSN 1463-5003, 2010.

Brooke, J. S. A. et al.: Meteoric smoke deposition in the polar regions: A comparison of measurements with global atmospheric models, *J. Geophys. Res.*, 122, pp. 11,112–11,130, 2017.

Carpenter, L. J., Fleming, Z. L., Read, K. A., Lee, J. D., Moller, S. J., Hopkins, J. R., Purvis, R. M., Lewis, A. C., Müller, K., Heinold, B., Herrmann, H., et al.: Seasonal characteristics of tropical marine boundary layer air measured at the Cape Verde Atmospheric Observatory, *Journal of Atmospheric Chemistry*, 67(2), pp.87-140. 2010.

Collins, W. J., Lamarque, J.-F., Schulz, M., Boucher, O., Eyring, V., Hegglin, M. I., Maycock, A., Myhre, G., Prather, M., Shindell, D., and Smith, S. J.: AerChemMIP: quantifying the effects of chemistry and aerosols in CMIP6, *Geosci. Model Dev.*, 10, 585–607, <https://doi.org/10.5194/gmd-10-585-2017>, 2017.

[Comiso, J. C., 2017: Bootstrap Sea Ice Concentrations from Nimbus-7 SMMR and DMSP SSM/I-SSMIS, Version 3, 1979–2022, Boulder, Colorado USA, NASA National Snow and Ice Data Center Distributed Active Archive Center, https://doi.org/10.5067/7Q8HCCWS4I0R.](https://doi.org/10.5067/7Q8HCCWS4I0R)

Coward, Andrew; Roberts, Malcolm (2018). *NERC HadGEM3-GC31-HH model output prepared for CMIP6 HighResMIP*. Version 20240131. Earth System Grid Federation. <https://doi.org/10.22033/ESGF/CMIP6.1822>

Daskalakis, N., Tsigaridis, K., Myriokefalitakis, S., Fanourgakis, G. S. and Kanakidou, M.: Large gain in air quality compared to an alternative anthropogenic emissions scenario. *Atmospheric Chemistry and Physics*, 16(15), pp.9771-9784, 2016.

Dee, D. P., Uppala, S. M., Simmons, A. J., Berrisford, P., Poli, P., Kobayashi, S., Andrae, U., Balmaseda, M. A., Balsamo, G., Bauer, P., Bechtold, P., Beljaars, A. C. M., van de Berg, L., Bidlot, J., Bormann, N., Delsol, C., Dragani, R., Fuentes, M., Geer, A. J., Haimberger, L., Healy, S. B., Hersbach, H., Hólm, E. V., Isaksen, I., Kållberg, P., Köhler, M., Matricardi, M., McNally, A. P., Monge-Sanz, B. M., Morcrette, J.-J., Park, B.-K., Peubey, C., de Rosnay, P., Tavolato, C., Thépaut, J.-N., and Vitart, F.: The ERA-Interim reanalysis: configuration and performance of the data assimilation system, *Q. J. Roy. Meteor. Soc.*, 137, 553–597, <https://doi.org/10.1002/qj.828>, 2011 (data available at: <https://www.ecmwf.int/en/forecasts/datasets/reanalysis-datasets/era-interim>, last access: 12 January 2023).

Dennison, F., Keeble, J., Morgenstern, O., Zeng, G., Abraham, N. L. and Yang, X.: Improvements to stratospheric chemistry scheme in the um-ukca (v10. 7) model: Solar cycle and heterogeneous reactions, *Geoscientific Model Development*, 12(3), pp.1227-1239. 2019.

[Desbruyères, D., McDonagh, E. L., King, B. A. and Thierry, V.: Global and full-depth ocean temperature trends during the early twenty-first century from Argo and repeat hydrography. *J. Climate*, 30, 1985–1997, 2017, doi:10.1175/JCLI-D-16-0396.1.](https://doi.org/10.1175/JCLI-D-16-0396.1)

Deleted: Bryden, H. L., Johns, W. E., King, B. A., McCarthy, G., McDonagh, E. L., Moat, B. I., Smeed, D. A.: Reduction in ocean heat transport at 26°N since 2008 cools the eastern subpolar gyre of the North Atlantic Ocean, *Journal of Climate*, 33 (5), 1677-1689. <https://doi.org/10.1175/JCLI-D-19-0323.1>, 2020.¶

Deleted: ¶

Dhomse, S.: *UMUKCA_Volcanic_Forcing_Data_Dhomse2020*, Mendeley Data, V1, <https://doi.org/10.17632/n3g2htz9hk.1>, 2020.

Dhomse, S. S. et al.: Aerosol microphysics simulations of Pinatubo eruption with UKCA composition-climate model, *Atmos. Chem. Phys.*, 14, pp. 11221–11246, 2014. <https://doi.org/10.5194/acp-14-11221-2014>, 2014.

Dhomse, S. S. et al.: Evaluating the simulated radiative forcings, aerosol properties, and stratospheric warmings from the 1963 Mt Agung, 1982 El Chichón, and 1991 Mt Pinatubo volcanic aerosol clouds, *Atmos. Chem. Phys.*, 20, 13627–13654, 2020, <https://doi.org/10.5194/acp-20-13627-2020>, 2020.

Dhomse, S., Feng, W., Rap, A., Carslaw, K., Bellouin, N., and Mann, G.: SMURPHS/ACSIS El Chichon volcanic forcing dataset (mapped to UM wavebands) -- from HErSEA ensemble of interactive strat-aerosol GA4 UM-UKCA runs (Dhomse et al., 2020, ACP) (Version v1) [Data set], Zenodo, <https://doi.org/10.5281/zenodo.4744634>, 2021a.

Dhomse, S., Feng, W., Rap, A., Carslaw, K., Bellouin, N., and Mann, G.: SMURPHS/ACSIS Agung volcanic forcing dataset (mapped to UM wavebands) -- from HErSEA ensemble of interactive strat-aerosol GA4 UM-UKCA runs (Dhomse et al., 2020, ACP) (Version v1) [Data set], Zenodo, <https://doi.org/10.5281/zenodo.4744687>, 2021b.

Drewnick, F., Hings, S. S., DeCarlo, P., Jayne, J. T., Gonin, M., Fuhrer, K., Weimer, S., Jimenez, J. L., Demerjian, K. L., Borrmann, S., and Worsnop, D. R.: A new time-of-flight aerosol mass spectrometer (TOF-AMS) – Instrument description and first field deployment, *Aerosol Sci. Tech.*, 39, 637–658, <https://doi.org/10.1080/02786820500182040>, 2005.

Dunstone, N. J., Smith, D. M., and Eade, R.: Multi-year predictability of the tropical Atlantic atmosphere driven by the high-latitude North Atlantic Ocean. *Geophys. Res. Lett.*, 38, L14701, <https://doi.org/10.1029/2011GL047949>, 2011.

Dussin, R., Barnier, B., Brodeau, L., and Molines, J. M.: The making of the DRAKKAR forcing set DFS5. DRAKKAR (MyOcean report 01-04-16), LGGE, Grenoble, France, 2016.

Facility for Airborne Atmospheric Measurements; Natural Environment Research Council; Met Office; Archibald, A.; Matthews, E.; Squires, F.; Wu, H.; Temple, L.: ACSIS: Merged airborne chemistry data from instruments on board the FAAM aircraft. NERC EDS Centre for Environmental Data Analysis, <https://doi:10.5285/6285564c34a246fc9ba5ce053d85e5e7>, 2024

Feng, W., Dhomse, S., Rap, A., Carslaw, K., Bellouin, N., and Mann, G.: SMURPHS/ACSIS Pinatubo volcanic forcing dataset (mapped to UM wavebands) -- from HErSEA ensemble of interactive strat-aerosol GA4 UM-UKCA runs (Dhomse et al., 2020, ACP) (v1), <https://doi.org/10.5281/zenodo.4739171>, 2021.

Good, S. A., Martin, M. J. and Rayner, N. A.: 2013. EN4: quality controlled ocean temperature and salinity profiles and monthly objective analyses with uncertainty estimates, *Journal of Geophysical Research: Oceans*, <https://doi.org/10.1002/2013JC009067>, 2013.

Griffies, S. M., Danabasoglu, G., Durack, P. J., Adcroft, A. J., Balaji, V., Böning, C. W., Chassignet, E. P., Curchitser, E., Deshayes, J., Drange, H., Fox-Kemper, B., Gleckler, P. J., Gregory, J. M., Haak, H., Hallberg, R. W., Heimbach, P., Hewitt, H. T., Holland, D. M., Ilyina, T., Jungclaus, J. H., Komuro, Y., Krasting, J. P., Large, W. G., Marsland, S. J., Masina, S., McDougall, T. J., Nurser, A. J. G., Orr, J. C., Pirani, A., Qiao, F., Stouffer, R. J., Taylor, K. E., Treguer, A. M., Tsujino, H., Uotila, P., Valdivieso, M., Wang, Q., Winton, M., and Yeager, S. G.: OMIP contribution to CMIP6: experimental and diagnostic protocol for the physical component

Deleted: Germe, A.; Hirschi, J. J.-M., Blaker, A. T., Sinha, B.: Chaotic variability of the Atlantic meridional overturning circulation at subannual time scales, *Journal of Physical Oceanography*, 52 (5), 929-949. <https://doi.org/10.1175/JPO-D-21-0100.1.2022>.[†]

of the Ocean Model Intercomparison Project, *Geosci. Model Dev.*, 9, 3231–3296, <https://doi.org/10.5194/gmd-9-3231-2016>, 2016.

Griffiths, P. T., Murray, L. T., Zeng, G., Shin, Y. M., Abraham, N. L., Archibald, A. T., Deushi, M., Emmons, L. K., Galbally, I. E., Hassler, B., Horowitz, L. W., Keeble, J., Liu, J., Moeini, O., Naik, V., O'Connor, F. M., Oshima, N., Tarasick, D., Tilmes, S., Turnock, S. T., Wild, O., Young, P. J., and Zanis, P.: Tropospheric ozone in CMIP6 simulations, *Atmos. Chem. Phys.*, 21, 4187–4218, <https://doi.org/10.5194/acp-21-4187-2021>, 2021.

Haarsma, R. J., Roberts, M. J., Vidale, P. L., Senior, C. A., Bellucci, A., Bao, Q., et al.: High Resolution Model Intercomparison Project (HighResMIP v1.0) for CMIP6, *Geoscientific Model Development*, 9(11), 4185–4208. <https://doi.org/10.5194/gmd-9-4185-2016>, 2016.

Helmig, D., Muñoz, M., Hueber, J., Mazzoleni, C., Mazzoleni, L., Owen, R.C., Val-Martin, M., Fialho, P., Plass-Duelmer, C., Palmer, P.I. and Lewis, A.C.: Climatology and atmospheric chemistry of the non-methane hydrocarbons ethane and propane over the North Atlantic NMHC at Pico Mountain, *Elementa: Science of the Anthropocene*, 3, 54, ISSN 2325-1026, 2015.

Helmig, D., Rossabi, S., Hueber, J. et al.: Reversal of global atmospheric ethane and propane trends largely due to US oil and natural gas production, *Nature Geosci* 9, 490–495, <https://doi.org/10.1038/ngeo2721>, 2016.

Hersbach, H., Bell, B., Berrisford, S., Hirahara, A., Horányi, J., Muñoz-Sabater, et al.: The ERA5 global reanalysis, *Q. J. R. Meteorol. Soc.*, 146, 1999–2049, 2020.

Hewitt, H. T., Hill, R. S., R. C. Copesey, D. Culverwell, I. D. Harris, C. M. Keen, A. B. McLaren, A. J. et al.: Design and implementation of the infrastructure of HadGEM3: the next generation Met Office climate modelling system. *Geoscientific Model Development*. 4(2), 2011.

Hirschi, J. J.-M., Barnier, B., Böning, C., Biastoch, A., Blaker, A. T., Coward, A., Danilov, S., Drijfhout, S., Getzlaff, K., Griffies, S. M., Hasumi, H., Hewitt, H., Iovino, D., Kawasaki, T., Kiss, A. E., Koldunov, N., Marzocchi, A., Mecking, J. V., Moat, B., Molines, J.-M., Myers, P. G., Penduff, T., Roberts, M., Treguier, A.-M., Sein, D. V., Sidorenko, D., Small, J., Spence, P., Thompson, L., Weijer, W., Xu, X.: The Atlantic meridional overturning circulation in high resolution models, *Journal of Geophysical Research: Oceans*, 125 (4), e2019JC015522. <https://doi.org/10.1029/2019JC015522>, 2020.

Huang, B., Thorne, P. W., et al.: Extended Reconstructed Sea Surface Temperature version 5 (ERSSTv5), Upgrades, validations, and intercomparisons, *J. Climate*, <https://doi.org/10.1175/JCLI-D-16-0836>, 2017.

Hunke, E. C., and Lipscomb, W. H.: Cice: The Los Alamos Sea ice model, documentation and software user's manual, version 4.1 (Tech. Rep.). Los Alamos National Laboratory, 2010.

Jackson, R. B. et al.: Increasing anthropogenic methane emissions arise equally from agricultural and fossil fuel sources, *Environ. Res. Lett.* 15, 071002, 2020.

Kanamitsu, M., et al.: NCEP–DOE AMIP-II reanalysis (R-2), *Bull. Amer. Meteor. Soc.*, **83**, 1631–1644, <https://doi.org/10.1175/BAMS-83-11-1631>, 2002.

Keeble, J., Hassler, B., Banerjee, A., Checa-Garcia, R., Chiodo, G., Davis, S., Eyring, V., Griffiths, P. T., Morgenstern, O., Nowack, P., Zeng, G., Zhang, J., Bodeker, G., Burrows, S., Cameron-Smith, P., Cugnet, D., Danek, C., Deushi, M., Horowitz, L. W., Kubin, A., Li, L., Lohmann, G., Michou, M., Mills, M. J., Nabat, P., Olivie, D., Park, S., Seland, Ø., Stoll, J., Wieners, K.-H., and Wu, T.: Evaluating stratospheric ozone and water vapour changes in CMIP6 models from 1850 to 2100, *Atmos. Chem. Phys.*, 21, 5015–5061, <https://doi.org/10.5194/acp-21-5015-2021>, 2021.

Deleted: Grist, J. P., Sinha, B., Hewitt, H. T., Duchez, A., MacLachlan, C., Hyder, P., Josey, S. A., Hirschi, J. J.-M., Blaker, A. T., New, A. L., Scaife, A. A., Roberts, C. D.: Re-emergence of North Atlantic subsurface ocean temperature anomalies in a seasonal forecast system. *Climate Dynamics*. 22, pp. <https://doi.org/10.1007/s00382-019-04826-w>, 2019.

Deleted: Josey, S. A. ; Sinha, B.: Subpolar Atlantic Ocean mixed layer heat content variability is increasingly driven by an active ocean, *Communications Earth & Environment*, 3 (1). <https://doi.org/10.1038/s43247-022-00433-6>, 2022.

Kennedy, J. J., Rayner, N. A., Atkinson, C. P., and Killick, R. E.: An ensemble data set of sea-surface temperature change from 1850: the Met Office Hadley Centre HadSST.4.0.0.0 data set, *Journal of Geophysical Research: Atmospheres*, 124. <https://doi.org/10.1029/2018JD029867>, 2019.

King B. A.: Objectively mapped Argo profiling float data and RAPID moored microcat data from the North Atlantic Ocean, 2004-2022. NERC EDS British Oceanographic Data Centre NOC. <https://doi.org/10.5285/fe8e524d-7f04-41f3-e053-6c86abc04d51>, 2023.

Kumar, A., Wu, S., Weise, M. F., Honrath, R., Owen, R. C., Helmig, D., Kramer, L., Val Martin, M. and Li, Q.: Free-troposphere ozone and carbon monoxide over the North Atlantic for 2001–2011: *Atmospheric Chemistry and Physics*, 13(24), 12537-12547, 2013.

Large, W. G., and Yeager, S. G.: The global climatology of an interannually varying air–sea flux data set, *Climate Dynamics*, 33(2), 341–364. <https://doi.org/10.1007/s00382-008-0441-3>, 2009.

Lawler, M. J. et al.: HOCl and Cl₂ observations in marine air, *Atmos. Chem. Phys.*, 11, 7617-7628. 2011.

Lee, B. H., Lopez-Hilfiker, F. D., Mohr, C., Kurtén, T., Worsnop, D. R., and Thornton, J. A.: An iodide-adduct high-resolution time-of-flight chemical-ionization mass spectrometer: Application to atmospheric inorganic and organic compounds, *Environmental science & technology*, 48(11), 6309-6317, 2018.

Loades, D. C., Yang, M., Bell, T. G., Vaughan, A. R., Pound, R. J., Metzger, S., Lee, J. D., and Carpenter, L. J.: Ozone deposition to a coastal sea: comparison of eddy covariance observations with reactive air-sea exchange models, *Atmos. Meas. Tech.*, 13, 6915-6931, [10.5194/amt-13-6915-2020](https://doi.org/10.5194/amt-13-6915-2020), 2020.

Lozier, M.S., Li, F., Bacon, S., Bahr, F., Bower, A., Cunningham, S., de Jong, F., de Steur, L., de Young, B., Fischer, J., Gary, S., Greenan, B., Holliday, N. P., Houk, A., Houpert, L., Inall, M., Johns, B., Johnson, H., Johnson, C., Karstensen, J., Koman, G., LeBras, I., Lin, X., Mackay, N., Marshall, D., Mercier, H., Oltmanns, M., Pickart, R., Ramsay, A., Rayner, D., Straneo, F., Thierry, V., Torres, D., Williams, R., Wilson, C., Yang, J., Yashayaev, I., Zhao, J.: A sea change in our view of overturning in the Subpolar North Atlantic Program, *Science* 01 Feb 2019:Vol. 363, Issue 6426, pp. 516-521 <https://doi.org/10.1126/science.aau6592>, 2019.

Luo, B.: Stratospheric aerosol data for use in CMIP6 models, available at: ftp://iacftp.ethz.ch/pub_read/luo/CMIP6/Readme_Data_Description.pdf, 2016 .

Madec et al.: NEMO ocean engine, Note du Poˆle de mode ´lisation de l’Institut Pierre-Simon Laplace No 27 ISSN No 1288-1619, 2016.

Madec, G., and the NEMO System Team: NEMO ocean engine, *Scientific Notes of Climate Modelling Center* (27) – ISSN 1288-1619, <https://doi.org/10.5281/zenodo.1464816>, 2019.

Mann, G. W. et al.: “Description and evaluation of GLOMAP-mode: a modal global aerosol microphysics model for the UKCA composition-climate model”, *Geosci. Mod. Dev.*, 3, 519–551, 2010, <https://doi.org/10.5194/gmd-3-519-2010>, 2010.

Mann, G. W. et al.: Evolving particle size is the key to improved volcanic forcings, *Past Global Change*, vol. 23, no. 2, 52-53, <https://doi.org/10.22498/pages.23.2.52>, 2015.

Matthews, E., Bannan, T. J., Khan, M. A. H., Shallcross, D. E., Stark, H., Browne, E. C., Archibald, A. T., Mehra, A., Bauguitte, S. J. B., Reed, C., Thamban, N. M., Wu, H., Barker, P.,

Lee, J., Carpenter, L. J., Yang, M., Bell, T. G., Allen, G., Jayne, J. T., Percival, C. J., McFiggans, G., Gallagher, M., Coe, H.: Airborne observations over the North Atlantic Ocean reveal the importance of gas-phase urea in the atmosphere. *National Academy of Sciences. Proceedings*, 120(25), Article e2218127120. <https://doi.org/10.1073/pnas.2218127120>, 2023

Matthews E, Examining novel atmospheric chemistry in the marine environment with an iodide chemical ionisation mass spectrometer. Ph. D. Thesis. The University of Manchester, 2023.

McCarthy, G. D., Smeed, D. A., Johns, W. E., Frajka-Williams, E., Moat, B. I. Rayner, D., Baringer, M.O., Meinen, C.S., Collins, J., Bryden, H.L.: Measuring the Atlantic Meridional Overturning Circulation at 26°N, *Progress in Oceanography*, 130: 91-111. <https://doi.org/10.1016/j.pocean.2014.10.006>, 2015.

McFiggans, G. B., et al.: Novel findings in the Reactive Halogens in the Marine Boundary Layer (RHAMBLE) project, *Geochimica Et Cosmochimica Acta*, 73, A857-A857, 2009.

Megann, A., Blaker, A., Josey, S., New, A., and Sinha, B.: Mechanisms for late 20th and early 21st Century decadal AMOC variability, *JGR: Oceans*, 126, e2021JC017865. <https://doi.org/10.1029/2021JC017865>, 2021a.

Megann, A., Sinha, B., and Blaker, A.: Monthly ocean and sea-ice output from 1/4° NEMO GO6 integration forced by CORE2 data, <https://doi.org/10/gm8vf7>, 2021b .

Megann, A., Sinha, B. and Blaker, A.: Monthly ocean and sea-ice output from 1/4° NEMO (GO6 integration forced by DFS5.2 data. NERC EDS British Oceanographic Data Centre. <https://doi.org/10/gm8vf5>, 2021c.

Megann, A., Sinha, B. and Blaker, A.: Monthly ocean and sea-ice output from 1/4° NEMO GO6 integration forced by JRA55 data. NERC EDS British Oceanographic Data Centre. <https://doi.org/10/gm8vf8>, 2021d.

Megann, A., Sinha, B., Blaker, A., Schroeder, D., Feltham, D.: The North Atlantic Climate System Integrated Study: model run output. NERC EDS British Oceanographic Data Centre NOC, accessed 27 March 2023, <http://catalogue.ceda.ac.uk/uuid/770a885a8bc34d51ad71e87ef346d6a8>, 2021e.

Megann, A., Blaker, A., Coward, A., Guiavarc'h, C., Storkey, D.: Model output from 1/4° global JRA55-forced integration of GO8p7 global ocean-sea ice model from 1958 to 2021, NERC British Oceanographic Data Centre, 20 October 2022. doi:10.5285/e02c8424657846468c1ff3a5acd0b1ab, 2022a.

Megann, A., Blaker, A., Coward, A., Guiavarc'h, C., Storkey, D.: Model output from 1/12° global JRA55-forced integration of GO8p7 global ocean-sea ice model from 1958 to 2021, NERC British Oceanographic Data Centre, 20 October 2022. doi:10.5285/399b0f762a004657a411a9ea7203493a, 2022b.

Middlebrook, A. M., Bahreini, R., Jimenez, J. L., and Canagaratna, M. R.: Evaluation of composition-dependent collection efficiencies for the aerodyne aerosol mass spectrometer using field data, *Aerosol Sci. Tech.*, 46, 258–271, <https://doi.org/10.1080/02786826.2011.620041>, 2012.

Moat, B. I.; Smeed, D. A.; Frajka-Williams, E.; Desbruyères, D. G.; Beaulieu, C.; Johns, W. E.; Rayner, D.; Sanchez-Franks, A.; Baringer, M. O.; Volkov, D.; Jackson, L. C.; Bryden, H. L.: Pending recovery in the strength of the meridional overturning circulation at 26° N, *Ocean Science*, 16 (4). 863-874. <https://doi.org/10.5194/os-16-863-2020>, 2020.

Deleted: Mecking, J. V., Drijfhout, S. S., Hirschi, J. J.-M., Blaker, A. T.: Ocean and atmosphere influence on the 2015 European heatwave, *Environmental Research Letters*, 14(11) 114035, <https://doi.org/10.1088/1748-9326/ab4d33>, 2019.¶

Deleted: Moat, B. I., Sinha, B., Josey, S. A., Robson, J., Ortega, P., Sévellec, F., Holliday, N. P., McCarthy, G. D., New, A. L., Hirschi, J. J.-M.: Insights into decadal North Atlantic sea surface temperature and ocean heat content variability from an eddy-permitting coupled climate model, *Journal of Climate*, 32(18). 6137-6161. <https://doi.org/10.1175/JCLI-D-18-0709.1>, 2019.¶

Moat, B.I.; King, B.A.; Macintosh, C.R. (2021a): Subpolar North Atlantic ocean heat content (surface to 1000m) using the EN4.2.2 temperature data set. NERC EDS British Oceanographic Data Centre NOC, <https://doi.org/10/g6wm>, 2021a

Moat, B. I., King, B. A., Macintosh, C. R.: Subpolar North Atlantic ocean heat content (surface to 1000m) using objectively mapped Argo profiling float data, NERC EDS British Oceanographic Data Centre NOC. <https://doi.org/10/g8g2>, 2021b.

Moat, B. I., Frajka-Williams, E., Smeed, D. A., Rayner, D., Johns, W. E., Baringer, M. O., Volkov, D., and Collins, J.: Atlantic meridional overturning circulation observed by the RAPID-MOCHA-WBTS (RAPID-Meridional Overturning Circulation and Heatflux Array-Western Boundary Time Series) array at 26N from 2004 to 2020 (v2020.2), British Oceanographic Data Centre - Natural Environment Research Council, UK. <https://doi.org/10.5285/e91b10af-6f0a-7fa7-e053-6c86abc05a09>, 2022.

Monks, P. S., Archibald, A. T., Colette, A., Cooper, O., Coyle, M., Derwent, R., Fowler, D., Granier, C., Law, K. S., Mills, G. E., Stevenson, D. S., Tarasova, O., Thouret, V., von Schneidemesser, E., Sommariva, R., Wild, O., and Williams, M. L.: Tropospheric ozone and its precursors from the urban to the global scale from air quality to short-lived climate forcer, *Atmos. Chem. Phys.*, 15, 8889–8973, <https://doi.org/10.5194/acp-15-8889-2015>, 2015.

Morgan, W. T., Allan, J. D., Bower, K. N., Capes, G., Crosier, J., Williams, P. I., and Coe, H.: Vertical distribution of sub-micron aerosol chemical composition from North-Western Europe and the North-East Atlantic, *Atmos. Chem. Phys.*, 9, 5389–5401, <https://doi.org/10.5194/acp-9-5389-2009>, 2009.

Mulcahy, J. P., Johnson, C., Jones, C. G., Povey, A. C., Scott, C. E., Sellar, A., Turnock, S. T., Woodhouse, M. T., Abraham, N. L., Andrews, M. B., Bellouin, N., Browse, J., Carslaw, K. S., Dalvi, M., Folberth, G. A., Glover, M., Grosvenor, D. P., Hardacre, C., Hill, R., Johnson, B., Jones, A., Kipling, Z., Mann, G., Mollard, J., O'Connor, F. M., Palmiéri, J., Reddington, C., Rumbold, S. T., Richardson, M., Schutgens, N. A. J., Stier, P., Stringer, M., Tang, Y., Walton, J., Woodward, S., and Yool, A.: Description and evaluation of aerosol in UKESM1 and HadGEM3-GC3.1 CMIP6 historical simulations, *Geosci. Model Dev.*, 13, 6383–6423, <https://doi.org/10.5194/gmd-13-6383-2020>, 2020.

National Centre for Atmospheric Science; Carpenter, L.J.; Hopkins, J.R.; Lewis, A.C.; Neves, L.M.; Moller, S.; Pilling, M.J.; Read, K.A.; Young, T.D.; Lee, J.D. (2010): Continuous Cape Verde Atmospheric Observatory Observations. NCAS British Atmospheric Data Centre, accessed 31 January, 2024. <http://catalogue.ceda.ac.uk/uuid/81693aad69409100b1b9a247b9ae75d5>.

Nisbet, E. G., Manning, M. R., Dlugokencky, E. J., Fisher, R. E., Lowry, D., Michel, S. E., Myhre, C. L., Platt, S. M., Allen, G., Bousquet, P. and Brownlow, R.: Very strong atmospheric methane growth in the 4 years 2014–2017: Implications for the Paris Agreement, *Global Biogeochemical Cycles*, 33(3), pp.318-342. 2019.

Oltmanns, M., Karstensen, J., Moore, G. W. K., and Josey, S. A.: Rapid cooling and increased storminess triggered by freshwater in the North Atlantic, *Geophysical Research Letters*, 47, e2020GL087207, <https://doi.org/10.1029/2020GL087207>, 2020.

Parrington, M., Palmer, P. I., Henze, D. K., Tarasick, D. W., Hyer, E. J., Owen, R. C., Helmig, D., Clerbaux, C., Bowman, K. W., Deeter, M. N., Barratt, E. M., Coheur, P.-F., Hurtmans, D., Jiang, Z., George, M., and Worden, J. R.: The influence of boreal biomass burning emissions on the distribution of tropospheric ozone over North America and the North Atlantic during 2010, *Atmos. Chem. Phys.*, 12, 2077–2098, <https://doi.org/10.5194/acp-12-2077-2012>, 2012.

Deleted: Monerie, P.-A., Robson, J., Dong, B. and Dunstone, N.: A role of the Atlantic Ocean in predicting summer surface air temperature over North East Asia? *Climate Dynamics*, 51 (1-2), pp. 473-491. ISSN 0930-7575, <https://doi.org/10.1007/s00382-017-3935-z>, 2018.

Phillips, D. P., Hopkins, F. E., Bell, T. G., Liss, P. S., Nightingale, P. D., Reeves, C. E., Wohl, C., and Yang, M.: Air–sea exchange of acetone, acetaldehyde, DMS and isoprene at a UK coastal site. *Atmos. Chem. Phys.*, 21, 10111–10132, <https://doi.org/10.5194/acp-21-10111-2021>, 2021.

Plymouth Marine Laboratory; Yang, M. (2017): Penlee Point Atmospheric Observatory: Meteorological and chemical observations 2014- present. Centre for Environmental Data Analysis, *accessed 31 January, 2024*. <https://catalogue.ceda.ac.uk/uuid/8f1ff8ea77534e08b03983685990a9b0>.

Prather, M. J., Zhu, X., Flynn, C. M., Strode, S. A., Rodriguez, J. M., Steenrod, S. D., Liu, J., Lamarque, J.-F., Fiore, A. M., Horowitz, L. W., Mao, J., Murray, L. T., Shindell, D. T., and Wofsy, S. C.: Global atmospheric chemistry – which air matters, *Atmos. Chem. Phys.*, 17, 9081–9102, <https://doi.org/10.5194/acp-17-9081-2017>, 2017.

Priestley, M., Le Breton, M., Bannan, T. J., Leather, K. E., Bacak, A., Reyes-Villegas, E., ... and Percival, C. J.: Observations of Isocyanate, Amide, Nitrate, and Nitro Compounds From an Anthropogenic Biomass Burning Event Using a ToF-CIMS, *Journal of Geophysical Research: Atmospheres*, 123(14), 7687-7704, 2018.

Ranjithkumar, A., Gordon, H., Williamson, C., Rollins, A., Pringle, K., Kupc, A., Abraham, N. L., Brock, C. and Carslaw, K.: Constraints on global aerosol number concentration, SO₂ and condensation sink in UKESM1 using ATom measurements, *Atmospheric Chemistry and Physics*, 21(6), pp.4979-5014. 2021.

Read K A. et al.: Extensive halogen-mediated ozone destruction over the tropical Atlantic Ocean, *Nature*, 453, 1232-1235. 2008.

Reeves, C. E., Penkett, S. A., Bauguitte, S., Law, K. S., Evans, M. J., Bandy, B. J., Monks, P. S., Edwards, G. D., Phillips, G., Barjat, H. and Kent, J.: Potential for photochemical ozone formation in the troposphere over the North Atlantic as derived from aircraft observations during ACSOE, *Journal of Geophysical Research: Atmospheres*, 107(D23), pp.ACH-14. 2002.

Reynolds, R. W., Rayner, N. A., Smith, T. M., Stokes, D. C. and Wang, W.: An improved in situ and satellite SST analysis for climate, *Journal of climate*, 15(13), pp.1609-1625. 2002.

Ridley, J. K., Blockley, E. W., Keen, A. B., Rae, J. G. L., West, A. E., and Schroeder, D., 2018: The sea ice model component of HadGEM3-GC3.1, *Geosci. Model Dev.*, 11, 713–723, <https://doi.org/10.5194/gmd-11-713-2018>. Roberts, Malcolm (2017a). *MOHC HadGEM3-GC31-MM model output prepared for CMIP6 HighResMIP highresSST-present*. Version 20240131. Earth System Grid Federation. <https://doi.org/10.22033/ESGF/CMIP6.6029>.

Roberts, Malcolm (2017b). *MOHC HadGEM3-GC31-HM model output prepared for CMIP6 HighResMIP highresSST-present*. Version 20240131. Earth System Grid Federation. <https://doi.org/10.22033/ESGF/CMIP6.6024>

Roberts, Malcolm (2018a). *MOHC HadGEM3-GC31-HM model output prepared for CMIP6 HighResMIP hist-1950*. Version 20240131. Earth System Grid Federation. <https://doi.org/10.22033/ESGF/CMIP6.6040>.

Roberts, Malcolm (2018b). *MOHC HadGEM3-GC31-HH model output prepared for CMIP6 HighResMIP control-1950*. Version 20240131. Earth System Grid Federation. <https://doi.org/10.22033/ESGF/CMIP6.5881>.

Roberts, Malcolm (2019a). *MOHC HadGEM3-GC31-MM model output prepared for CMIP6 HighResMIP highresSST-future*. Version 20240131. Earth System Grid Federation. <https://doi.org/10.22033/ESGF/CMIP6.6013>.

Formatted: Space After: 6 pt

Deleted: ¶

Reed, C., Evans, M. J., Crilley, L. R., Bloss, W. J., Sherwen, T., Read, K. A., Lee, J. D., and Carpenter, L. J.: Evidence for renoxification in the tropical marine boundary layer, *Atmos. Chem. Phys.*, 17, 4081–4092, <https://doi.org/10.5194/acp-17-4081-2017>, 2017. ¶

Roberts, Malcolm (2019b). *MOHC HadGEM3-GC31-HM model output prepared for CMIP6 HighResMIP highresSST-future*. Version 20240131. Earth System Grid Federation. <https://doi.org/10.22033/ESGF/CMIP6.6008>.

Roberts, Malcolm (2019c). *MOHC HadGEM3-GC31-HM model output prepared for CMIP6 HighResMIP highres-future*. Version 20240131. Earth System Grid Federation. <https://doi.org/10.22033/ESGF/CMIP6.5984>.

Roberts, M. J., Vidale, P. L., Senior, C., Hewitt, H. T., Bates, C., Berthou, S., et al.: The Benefits of Global High Resolution for Climate Simulation: Process Understanding and the Enabling of Stakeholder Decisions at the Regional Scale, *Bulletin of the American Meteorological Society*, 99(11), 2341–2359. <https://doi.org/10.1175/BAMS-D-15-00320.1>, 2018.

Roberts, M. J., Baker, A., Blockley, E. W., Calvert, D., Coward, A., Hewitt, H. T., et al.: Description of the resolution hierarchy of the global coupled HadGEM3-GC3.1 model as used in CMIP6 HighResMIP experiments, *Geoscientific Model Development*, 12(12), 4999–5028. <https://doi.org/10.5194/gmd-12-4999-2019>, 2019.

Roberts, M. J., Jackson, L. C., Roberts, C. D., Meccia, V., Docquier, D., Koenigk, T., Ortega, P., Moreno-Chamarro, E., Bellucci, A., Coward, A., Drijfhout, S., Exarchou, E.,; Gutjahr, O., Hewitt, H., Iovino, D., Lohmann, K., Putrasahan, D., Schiemann, R., Seddon, J., Terray, L., Xu, X., Zhang, Q., Chang, P., Yeager, S. G., Castruccio, F. S., Zhang, S., Wu, L.: Sensitivity of the Atlantic meridional overturning circulation to model resolution in CMIP6 HighResMIP simulations and implications for future changes. *Journal of Advances in Modeling Earth Systems*, 12 (8), e2019MS002014, <https://doi.org/10.1029/2019MS002014>, 2020.

Robson, J., Sutton, R. T., Archibald, A., Cooper, F., Christensen, M., Gray, L. J., Holliday, N. P., Macintosh, C., McMillan, M., Moat, B., Russo, M., Tilling, R., Carslaw, K., Desbruyères, D., Embury, O., Feltham, D. L., Grosvenor, Daniel P., Josey, S., King, B., Lewis, A., McCarthy, G. D., Merchant, C., New, A. L., O'Reilly, C. H., Osprey, S. M., Read, K., Scaife, A., Shepherd, A., Sinha, B., Smeed, D., Smith, D., Ridout, A., Woollings, T., Yang, M.: Recent multivariate changes in the North Atlantic climate system, with a focus on 2005-2016, *International Journal of Climatology*, 38 (14), 5050-5076, <https://doi.org/10.1002/joc.5815>, 2018.

Robson, J., Aksenov, Y., Bracegirdle, T. J., Dimdore-Miles, O., Griffiths, P. T., Grosvenor, D. P., Hodson, D. L. R., Keeble, J., Megann, A., Osprey, S., Povey, A. C., Schröder, D., Yang, M., Archibald, A. T., Carslaw, K. S., Gray, L., Jones, C., Kerridge, B., Knappett, D., Kuhlbrodt, T., Russo, M., Sellar, A., Siddans, R., Sinha, B., Sutton, R., Walton, J., Wilcox, L. J.: The evaluation of the North Atlantic climate system in UKESM1 historical simulations for CMIP6, *Journal of Advances in Modeling Earth Systems*, 12 (9), e2020MS002126. <https://doi.org/10.1029/2020MS002126>, 2020.

Rollins, A. W., Thornberry, T. D., Ciciora, S. J., McLaughlin, R. J., Watts, L. A., Hanisco, T. F., Baumann, E., Giorgetta, F. R., Bui, T. V., Fahey, D. W., and Gao, R.-S.: A laser-induced fluorescence instrument for aircraft measurements of sulfur dioxide in the upper troposphere and lower stratosphere, *Atmos. Meas. Tech.*, 9, 4601–4613, <https://doi.org/10.5194/amt-9-4601-2016>, 2016

Russo, M. R., Kerridge, B. J., Abraham, N. L., Keeble, J., Latter, B. G., Siddans, R., Weber, J., Griffiths, P. T., Pyle, J. A., and Archibald, A. T.: Seasonal, interannual and decadal variability of tropospheric ozone in the North Atlantic: comparison of UM-UKCA and remote sensing observations for 2005–2018, *Atmos. Chem. Phys.*, 23, 6169–6196, <https://doi.org/10.5194/acp-23-6169-2023>, 2023.

Schiemann, R.; Vidale, P.; Hatcher, R.; Roberts, M. (2019a). *NERC HadGEM3-GC31-HM model output prepared for CMIP6 HighResMIP hist-1950*. Version 20240131. Earth System Grid Federation. <https://doi.org/10.22033/ESGF/CMIP6.6041>.

Schiemann, R.; Vidale, P. L.; Hatcher, R.; Roberts, M. (2019b). *NERC HadGEM3-GC31-HM model output prepared for CMIP6 HighResMIP highres-future*. Version 20240131. Earth System Grid Federation. <https://doi.org/10.22033/ESGF/CMIP6.5985>.

Schroeder, D., Feltham, D. L., Tsamados, M., Ridout, A. and Tilling, R.: New insight from CryoSat-2 sea ice thickness for sea ice modelling, *The Cryosphere* 13(1), 125-139. ISSN 1994-0424. <https://doi.org/10.5194/tc-13-125-2019>, 2019.

Sellar, A. A., Jones, C. G., Mulcahy, J. P., Tang, Y., Yool, A., Wiltshire, A., O'Connor, F. M., Stringer, M., Hill, R., Palmieri, J., Woodward, S., de Mora, L., Kuhlbrodt, T., Rumbold, S. T., Kelley, D. I., Ellis, R.; Johnson, C. E., Walton, J., Abraham, N. L., Andrews, M. B., Andrews, T., Archibald, A. T., Berthou, S., Burke, E., Blockley, E., Carslaw, K., Dalvi, M., Edwards, J., Folberth, G. A., Gedney, N., Griffiths, P. T., Harper, A. B., Hendry, M. A., Hewitt, A. J., Johnson, B., Jones, A., Jones, C. D., Keeble, J., Liddicoat, S., Mordenstern, O., Parker, R. J., Predoi, V., Robertson, E., Siahann, A., Smith, R. S., Swaminathan, R., Woodhouse, M. T., Zeng, G., Zerroukat, M.: UKESM1: description and evaluation of the U.K. Earth System Model, *Journal of Advances in Modeling Earth Systems*, 11 (12). 4513-4558. <https://doi.org/10.1029/2019MS001739>, 2019.

Sinclair, K., van Dierenhoven, B., Cairns, B., Alexandrov, M., Moore, R., Ziemba, L. D. and Crosbie, E.: Observations of aerosol-cloud interactions during the North Atlantic aerosol and marine ecosystem study, *Geophysical Research Letters*, 47(3), p.e2019GL085851. 2020.

Smyth, T. (2024): ACSIS: Sunphotometer aerosol measurements at Plymouth Marine Laboratory - Version 1. 2001-2023. NERC EDS Centre for Environmental Data Analysis, accessed 31 January, 2024, <https://catalogue.ceda.ac.uk/uuid/e74491c96ef24df29a9342a3d57b5939>

Sommariva, R., Hollis, L. D. J., Sherwen, T., et al.: Seasonal and geographical variability of nitryl chloride and its precursors in Northern Europe, *Atmos Sci Lett.*, 19 (8), <https://doi.org/10.1002/asl.844>, 2018.

Storkey, D., Blaker, A. T., Mathiot, P., Megann, A., Aksenov, Y., Blockley, E. W., Calvert, D., Graham, T., Hewitt, H. T., Hyder, P., Kuhlbrodt, T., Rae, J. G. L., and Sinha, B.: UK Global Ocean GO6 and GO7: a traceable hierarchy of model resolutions, *Geosci. Model Dev.*, 11, 3187–3213, <https://doi.org/10.5194/gmd-11-3187-2018>, 2018.

Sutton, R. T., McCarthy, G. D., Robson, J., Sinha, B., Archibald, A. T. and Gray, L. J.: Atlantic multidecadal variability and the UK ACSIS program, *Bulletin of the American Meteorological Society*, 99(2), 415-425, 2018.

Telford, P. J., Braesicke, P., Morgenstern, O. and Pyle, J. A.: Description and assessment of a nudged version of the new dynamics Unified Model, *Atmospheric Chemistry and Physics*, 8(6), 1701-1712, 2008.

Thompson, R. L. et al.: Variability in atmospheric methane from fossil fuel and microbial sources over the last three decades, *Geophys. Res. Lett.*, 45, 11499–11508, 2018.

Tilling, R. L., Ridout, A. and Shepherd, A.: Estimating Arctic sea ice thickness and volume using CryoSat-2 radar altimeter data. *Advances in Space Research*, 62(6), pp.1203-1225, 2018.

Deleted: ¶

Deleted: Schultz, M. G., Schröder, S., Lyapina, O., Cooper, O. R., Galbally, I., Petropavlovskikh, I., Von Schneidmesser, E., Tanimoto, H., Elshorbany, Y., Naja, M. and Seguel, R. J. et al.: Tropospheric Ozone Assessment Report: Database and metrics data of global surface ozone observations, *Elementa: Science of the Anthropocene*, 5, 58, <https://doi.org/10.1525/elementa.244>, 2017. ¶

Deleted: Smeed, D. A., Josey, S. A., Beaulieu, C., Johns, W. E., Moat, B. I., Frajka-Williams, E., Rayner, D., Meinen, C. S., Baringer, M. O., Bryden, H. L., and McCarthy, G. D.: The North Atlantic Ocean is in a state of reduced overturning, *Geophysical Research Letters*, 45 (3), 1527-1533, <https://doi.org/10.1002/2017GL076350>, 2018. ¶

Timmreck, C. et al.: The Interactive Stratospheric Aerosol Model Intercomparison Project (ISA-MIP): motivation & experiment design, *Geosci. Mod. Dev.*, 11, 2581-2608, <https://doi.org/10.5194/gmd-11-2581-2018>, 2018.

Tsujino, H., et al.: JRA-55 based surface dataset for driving ocean-sea ice models (JRA55-do) Ocean Modelling, 130, 79-139, <https://doi.org/10.1016/j.ocemod.2018.07.002>, 2018.

Turnock, S. T., Butt, E. W., Richardson, T. B., Mann, G. W., Reddington, C. L., Forster, P. M., Haywood, J., Crippa, M., Janssens-Maenhout, G., Johnson, C. E. and Bellouin, N.: The impact of European legislative and technology measures to reduce air pollutants on air quality, human health and climate, *Environmental Research Letters*, 11(2), p.024010, 2016.

Turnock, S. T., Allen, R. J., Andrews, M., Bauer, S. E., Deushi, M., Emmons, L., Good, P., Horowitz, L., John, J. G., Michou, M., Nabat, P., Naik, V., Neubauer, D., O'Connor, F. M., Olivie, D., Oshima, N., Schulz, M., Sellar, A., Shim, S., Takemura, T., Tilmes, S., Tsigaridis, K., Wu, T., and Zhang, J.: Historical and future changes in air pollutants from CMIP6 models, *Atmos. Chem. Phys.*, 20, 14547–14579, <https://doi.org/10.5194/acp-20-14547-2020>, 2020.

Van Pinxteren et al.: Marine organic matter in the remote environment of the Cape Verde islands – an introduction and overview to the MarParCloud campaign, *ACP*, acp-2019-997, 2020.

Walters, D. et al.: The Met Office Unified Model Global Atmosphere 4.0 and JULES Global Land 4.0 configurations, *Geosci. Model Dev.*, 7, 361–386, <https://doi.org/10.5194/gmd-7-361-2014>, 2014.

White, C., Ussher, S. J., Fitzsimons, M. F., Atkinson, S., Woodward, E. M. S., Yang, M., Bell, T. G.: Inorganic nitrogen and phosphorus in Western European aerosol and the significance of dry deposition flux into stratified shelf waters, *Atmospheric Environment*, 261, 118391, <https://doi.org/10.1016/j.atmosenv.2021.118391>, 2021.

Williams, K. D., Copsey, D., Blockley, E. W., Bodas-Salcedo, A., Comer, C. R., Davis, P., et al.: The Met Office Global Coupled Model 3.0 and 3.1 (GC3.0 and GC3.1) Configurations, *Journal of Advances in Modeling Earth Systems*, 10, 357–380, <https://doi.org/10.1002/2017MS001115>, 2017.

Williams, S. D. P., and Berry, D. I.: ACSIS Atlantic Ocean medium resolution SST dataset: Reconstructed 5-day, ½-degree, Atlantic Ocean SST (1950-2014). *Geoscience Data Journal*, 7 (2), 135-148, <https://doi.org/10.1002/gdj3.94>, 2020.

Wilkinson, M. D., Dumontier, M., Aalbersberg, I. J., Appleton, G., Axton, M., Baak, A., Blomberg, N., Boiten, J. W., da Silva Santos, L. B., Bourne, P. E. and Bouwman, J.: The FAIR Guiding Principles for scientific data management and stewardship. *Scientific data*, 3(1), 1-9, 2016.

Wofsy, S. C., Afshar, S., Allen, H. M., Apel, E., Asher, E. C., Barletta, B., Bent, J., Bian, H., Biggs, B. C., Blake, D. R., Blake, N., Bourgeois, I., Brock, C. A., Brune, W. H., Budney, J. W., Bui, T. P., Butler, A., Campuzano-Jost, P., Chang, C. S., Chin, M., Commane, R., Correa, G., Crouse, J. D., Cullis, P. D., Daube, B. C., Day, D. A., Dean-Day, J. M., Dibb, J. E., DiGangi, J. P., Diskin, G. S., Dollner, M., Elkins, J. W., Erdesz, F., Fiore, A. M., Flynn, C. M., Froyd, K., Gesler, D. W., Hall, S. R., Hanisco, T. F., Hannun, R. A., Hills, A. J., Hints, E. J., Hoffman, A., Hornbrook, R. S., Huey, L. G., Hughes, S., Jimenez, J. L., Johnson, B. J., Katich, J. M., Keeling, R. F., Kim, M. J., Kupc, A., Lait, L. R., Lamarque, J.-F., Liu, J., McKain, K., Mclaughlin, R. J., Meinardi, S., Miller, D. O., Montzka, S. A., Moore, F. L., Morgan, E. J., Murphy, D. M., Murray, L. T., Nault, B. A., Neuman, J. A., Newman, P. A., Nicely, J. M., Pan, X., Paplawsky, W., Peischl, J., Prather, M. J., Price, D. J., Ray, E., Reeves, J. M., Richardson, M., Rollins, A. W., Rosenlof, K. H., Ryerson, T. B., Scheuer, E., Schill, G. P., Schroder, J. C., Schwarz, J. P., St. Clair, J. M., Steenrod, S. D., Stephens, B. B., Strode, S. A., Sweeney, C., Tanner, D., Teng, A.

P., Thames, A. B., Thompson, C. R., Ullmann, K., Veres, P. R., Vieznor, N., Wagner, N. L., Watt, A., Weber, R., Weinzierl, B., Wennberg, P., Williamson, C. J., Wilson, J. C., Wolfe, G. M., Woods, C. T., and Zeng, L. H.: *ATom: Merged Atmospheric Chemistry, Trace Gases, and Aerosols*, ORNL DAAC, Oak Ridge, Tennessee, USA, 10.3334/ORNLDAAC/1581, 2018.

Yang, M. and Fleming, Z. L.: Estimation of atmospheric total organic carbon (TOC)—paving the path towards carbon budget closure, *Atmospheric Chemistry and Physics*, 19(1), 459–471. 2019.

Yang, M., Bell, T. G., Hopkins, F. E., and Smyth, T. J.: Attribution of atmospheric sulfur dioxide over the English Channel to dimethyl sulfide and changing ship emissions, *Atmos. Chem. Phys.*, 16, 4771–4783, <https://doi.org/10.5194/acp-16-4771-2016>, 2016a.

Yang, M., Bell, T. G., Hopkins, F. E., Kitidis, V., Cazenave, P. W., Nightingale, P. D., Yelland, M. J., Pascal, R. W., Prytherch, J., Brooks, I. M., and Smyth, T. J.: Air-sea fluxes of CO₂ and CH₄ from the Penlee Point Atmospheric Observatory on the south-west coast of the UK, *Atmospheric Chemistry and Physics*, 16, 5745–5761, <https://doi.org/10.5194/acp-16-5745-2016>, 2016b.

Yang, M., Prytherch, J., Kozlova, E., Yelland, M. J., Parenkat Mony, D., and Bell, T. G.: Comparison of two closed-path cavity-based spectrometers for measuring air–water CO₂ and CH₄ fluxes by eddy covariance, *Atmos. Meas. Tech.*, 9, 5509–5522, <https://doi.org/10.5194/amt-9-5509-2016>, 2016c.

Yang, M., Bell, T. G., Hopkins, F. E., and Smyth, T. J.: Attribution of atmospheric sulfur dioxide over the English Channel to dimethyl sulfide and changing ship emissions, *Atmospheric Chemistry and Physics*, 16, 4771–4783, <https://doi.org/10.5194/acp-16-4771-2016>, 2016d.

Yang, M., Bell, T. G., Brown I. J., Fishwick J. R., Kitidis, V., Nightingale, P. D., Rees, A. P., and Smyth T. J.: Insights from year-long measurements of air–water CH₄ and CO₂ exchange in a coastal environment, *Biogeosciences*, 16, 961–978, <https://doi.org/10.5194/bg-16-961-2019a>, 2019a.

Yang, M., Norris, S. J., Bell, T. G., and Brooks, I. M.: Sea spray fluxes from the southwest coast of the United Kingdom dependence on wind speed and wave height. *Atmos. Chem. Phys.*, 19, 15271–15284, <https://doi.org/10.5194/acp-19-15271-2019>, 2019b.

Zawadowicz, M. A., Suski, K., Liu, J., Pekour, M., Fast, J., Mei, F., Sedlacek, A. J., Springston, S., Wang, Y., Zaveri, R. A., Wood, R., Wang, J., and Shilling, J. E.: Aircraft measurements of aerosol and trace gas chemistry in the eastern North Atlantic, *Atmos. Chem. Phys.*, 21, 7983–8002, <https://doi.org/10.5194/acp-21-7983-2021>, 2021.